

RESEARCH

Open Access



# Identification and validation of an endoplasmic reticulum stress related model to predict prognosis and tumor microenvironment in neuroblastoma

Ji Chen<sup>1</sup>, Baofeng Du<sup>1\*</sup>, Bin Jiang<sup>1\*</sup> and Lei Huang<sup>1\*</sup>

## Abstract

**Background** This study investigated endoplasmic reticulum(ER) stress mechanisms in Neuroblastoma(NB) progression using bioinformatics and experimental validation.

**Methods** Using GSE49710 and E-MTAB-8248 datasets, ER stress related genes(ERSRGs) were analyzed. Consensus clustering identified ER stress related subtypes(ERSRsubtype). Integrated bioinformatic analyses identified key hub genes, dysregulated biological pathways, and significant alterations in immune cell infiltration within the studied context. A prognostic model was constructed via least absolute shrinkage and selection operator(LASSO)/multivariate regression and validated across multiple datasets. Drug sensitivity and microenvironment differences were assessed. Lentiviral knockdown, Cell Counting Kit-8(CCK8), 5-Ethynyl'-2-deoxyuridine(EdU), and Transwell assays evaluated *HIST1H1B*'s roles in NB cell lines.

**Result** 173 prognosis-linked ESRGs were identified. The samples were stratified into two ERSRsubtypes with distinct prognoses. We obtained 4 hub genes and multiple differentially expressed pathways in the two subtypes. The ER stress related model accurately predicted survival. High-risk patients showed altered immune infiltration(8 cell types) and 149 differentially effective drugs(18 more effective in high-risk NB). *HIST1H1B*, upregulated in *MYCN*-amplified NB, enhanced proliferation, migration, and invasion of NB.

**Conclusion** ERSRsubtypes were associated with NB prognosis and tumor microenvironment(TME) heterogeneity. The prognostic model and key genes identified provide crucial insights into ER stress mechanisms, offering potential targets for therapy and aiding in risk stratification and treatment strategy formulation.

**Keywords** Neuroblastoma, Endoplasmic reticulum, Prognostic model, Immune infiltration, Chemotherapeutic response

\*Correspondence:

Baofeng Du

aduetty@163.com

Bin Jiang

jiangbin363@163.com

Lei Huang

surgeonhuang@126.com

<sup>1</sup>Department of General Surgery, Children's Hospital of Nanjing Medical University, Nanjing 210008, China



© The Author(s) 2026. **Open Access** This article is licensed under a Creative Commons Attribution-NonCommercial-NoDerivatives 4.0 International License, which permits any non-commercial use, sharing, distribution and reproduction in any medium or format, as long as you give appropriate credit to the original author(s) and the source, provide a link to the Creative Commons licence, and indicate if you modified the licensed material. You do not have permission under this licence to share adapted material derived from this article or parts of it. The images or other third party material in this article are included in the article's Creative Commons licence, unless indicated otherwise in a credit line to the material. If material is not included in the article's Creative Commons licence and your intended use is not permitted by statutory regulation or exceeds the permitted use, you will need to obtain permission directly from the copyright holder. To view a copy of this licence, visit <http://creativecommons.org/licenses/by-nc-nd/4.0/>.

## Introduction

NB is the most common extracranial solid tumor in children [1], and its unique and variable clinical features pose a significant challenge in diagnosing and treating NB [2]. The age, international neuroblastoma staging system (INSS) stage, imaging risk stratification, pathological type, and biological characteristics (*MYCN* amplification, chromosomal ploidy, 1p and 11q deletion) are important factors that influence the staging of NB [2–4]. For low or intermediate-risk NB, surgery alone or combined with chemotherapy can achieve a favorable prognosis [5]. However, for high-risk NB, even with intensive multimodal therapies such as induction chemotherapy [6, 7], surgery, radiation [8, 9], autologous stem cell transplantation [10–12], and immunotherapy [12–15], the 5-year survival rate remains low. Therefore, in-depth research on the occurrence and development of NB, especially the mechanisms of disease progression, will provide new insights for the treatment of high-risk NB.

The ER is an important organelle in eukaryotic cells, playing a crucial role in protein synthesis, folding, modification, calcium storage, and lipid synthesis [16]. Therefore, maintaining the homeostasis of the ER is a prerequisite for cells to carry out normal biological functions. Tumors, characterized by strong metabolic abilities and fast proliferation rates, require rapid expansion of the ER, which leads to a TME characterized by hypoxia, acidosis, and glucose deprivation [17, 18]. This environment causes the accumulation of newly synthesized unfolded proteins in the ER of tumor cells, ultimately triggering the ER stress response [19]. Studies have shown that ER stress response is associated with a large number of solid tumors [20–23], and that ER stress response and the unfolded protein response (UPR) play important roles in tumor occurrence and development, and targeting ER stress related pathways can significantly inhibit the occurrence and development of NB. Currently, only a few studies have found that the malignant progression of NB is closely related to ER stress [24–25], and the UPR is crucial for NB to adapt to the occurrence and development of *MYCN*-driven NB [25].

Currently, there is a lack of systematic literature that comprehensively elucidates the role of ER stress in the occurrence and development of NB. The relationship between the ER stress and the TME of NB is also unclear. In this study, we divided NB samples into different subtypes associated with ER stress using chip data from the Gene Expression Omnibus (GEO) (<https://www.ncbi.nlm.nih.gov/geo/>), ArrayExpress (<https://www.ebi.ac.uk/biostudies/arrayexpress>), and Therapeutically Applicable Research to Generate Effective Treatments (TARGET) databases (<https://www.cancer.gov/ccg/>). We then analyzed the differences in hub genes, pathways, and TME between these subtypes using weighted gene

co-expression network analysis (WGCNA), gene set enrichment analysis (GSEA) and gene set variation analysis (GSVA). Additionally, we constructed a reliable ER stress related prognostic model for NB and confirmed its significant guidance in evaluating prognosis and predicting drug sensitivity of NB.

## Materials and methods

### Data collection

This study included chip data from the GSE49710, GSE16476, GSE89413, E-MTAB-8248 datasets, and the TARGET database, which comprised chip data from 154 NB patients. The main clinical information collected included age, gender, *MYCN* status, INSS stage, Children's Oncology Group (COG) risk, overall survival status, and overall survival day. After data correction and probe annotation, a chip matrix data was obtained, with gene names as row names and patient/cell line numbers as column names. The GSE49710 and E-MTAB-8248 datasets were standardized using the “normalizeBetweenArrays()” function and then merged [26].

### Screening for ESRGs associated with NB prognosis

We obtained ESRGs from the Human Gene Set: “SetGOBP\_RESPONSE\_TO\_ENDOPLASMIC\_RETICULUM\_STRESS” in the MSigDB database. By taking the intersection with all genes in the merged cohort, ESRGs were eventually obtained for further study. In this study, univariate cox regression analysis was performed on the combined cohort ( $HR \neq 1$ ,  $p < 0.05$ ) to screen for ESRGs closely related to survival status of children with NB.

### Consensus clustering analysis for ESRGs

After performing consensus clustering analysis on the 721 NB samples using the “ConsensusClusterPlus()” function with parameters  $reps = 50$ ,  $pItem = 0.8$ ,  $pFeature = 1$ ,  $clusterAlg = "km"$ ,  $distance = "euclidean"$ ,  $seed = 123$ , the optimal clustering value of  $k$  was determined based on the results obtained from analyzing the expression levels of ESRGs closely associated with the prognosis of NB patients. Principal component analysis (PCA) was conducted on the 721 NB samples using the “prcomp()” function, and Kaplan-Meier (KM) survival analysis was performed on the different ESR-subtypes identified from consensus clustering analysis. The differential expression of ESRGs in the different ESR-subtypes was assessed using the “Lima” package, applying the criteria of  $|\log_2 FC| > 0.5$  and  $p < 0.05$ . The resulting differentially expressed genes (DEGs) were then visualized through the “ggboxplot()” and “pheatmap()” functions, displaying the expression levels of ESRGs in the different subtypes respectively.

### GSEA and GSVA

In this study, two hallmark gene sets, “c5.go.v7.4.symbols.gmt” and “c2.cp.kegg.v7.4.symbols.gmt”, were obtained from the MSigDB database. The “GSVA” R package and the “GSEA” function were used for GSVA and GSEA enrichment analysis respectively. The “pheatmap()” function and the “gseaplot2()” function were utilized for data visualization.

### Analysis of the differences in TME between two subtypes

Single-sample gene set enrichment analysis (SsGSEA) and cell-type identification by estimating relative subsets of RNA transcripts (CIBERSORT) were utilized to calculate the disparities in immune cell infiltration among various ERSRsubtypes/risk groups. The “GSVA()” function and the “CIBERSORT()” function were employed to determine immune scores for each sample. The “ggboxplot()” function and the “corrplot()” function were utilized to visually illustrate the correlation between immune cells in different subtypes/risk groups. The association between immune cells and hub genes/risk scores was analyzed using the “Cor.test()” function.

### WGCNA

To identify core genes with differential expression between different ERSRsubtypes, we performed WGCNA analysis on the merged chip matrix data. After applying a filtering criterion of Height = 2000 to remove outliers, we proceeded to perform hierarchical clustering analysis on the remaining samples using the “hclust()” function, followed by visualization of the clustering results in the form of a dendrogram. In order to minimize errors and ensure the biological significance of our analysis, we employed the “pickSoftThreshold()” function to carefully select an optimal soft threshold. Our goal was to achieve an approximate scale-free network with a criterion of  $R^2 > 0.85$ , thereby guaranteeing that the network followed a power-law distribution. We obtained multiple significant modules by applying the dynamic tree-cutting method to merge modules with high similarity, using a threshold of 0.25 for the cut height and a minimum gene number of 50. Gene significance (GS) was used to assess the correlation between genes and samples, and the module significance was calculated as the average GS of all genes within the module. The key module, which displayed the highest correlation, was identified. We calculated the GS and module membership (MM) for each gene in the key module and set a cut-off of  $GS > 0.5$  and  $MM > 0.80$  to obtain the core genes of the key module. By taking the intersection of previously identified DEGs and core genes, we obtained the hub genes closely associated with ER stress in NB.

### Development and reliability evaluation of prognosis related signature

The samples were randomly and evenly divided into training group and testing group. LASSO regression analysis was performed on the selected ERSRGs using the “Glmnet()” function, resulting in the identification of highly correlated genes with ERSRsubtypes and the minimum regularization parameter  $\lambda$  [27]. Core genes and their corresponding coefficients were then screened through multivariate cox regression analysis. The risk score for each sample was calculated using the obtained formula. Subsequently, the samples were categorized into high-risk and low-risk groups according to the median risk score. KM survival analysis was conducted to evaluate the survival outcomes between different risk groups. To analyze various parameters, such as receiver operating characteristic (ROC) curve, cox regression analysis, calibration curve, cumulative risk curve, and decision curve, the functions “pROC()”, “coxp()”, “calibrate()”, “survfit()”, and “dca()” were utilized.

### Drug sensitivity analysis

The training set gene expression matrix file “GDSC2\_Expr.rds” and drug treatment information file “GDSC2\_Res.rds” used for drug sensitivity analysis were obtained from the Genomics of Drug Sensitivity in Cancer database (<https://www.cancerrxgene.org/>). We selected the important function “calcPhenotype()” from the “oncoPredict” R package and set the criteria of removeLowVaryingGenes = 0.2 and minNumSamples = 10 to predict drug sensitivity.

### Cell culture and authentication

All NB cell lines including SK-N-SH, SH-SY5Y, SK-N-BE(2), BE(2)-117, KPNYN, IMR-32, and SK-N-DZ were procured from the American Type Culture Collection, with the exception of the Kelly cell line which was generously provided by Dr. Qing Guoliang (Department of Pathophysiology, Wuhan University School of Basic Medicine). SK-N-SH, SH-SY5Y, SK-N-BE(2), BE(2)-117, KPNYN, IMR-32 and SKNDZ were cultured with DMEM (Gibco, USA) supplemented with 10% fetal bovine serum (Gibco, USA) and 1% Penicillin/Streptomycin (New cell & Molecular Biotech, China). Kelly cell line was grown in complete RPMI-1640 (Gibco, USA) supplemented with 10% FBS and 1% penicillin/streptomycin. All cell stocks were authenticated through short tandem repeat profiling using the CellCheck® 9-marker system (IDEXX, USA) and confirmed mycoplasma-free via MycoAlert™ PLUS detection kit (Lonza, Switzerland), with strict adherence to 6-month post-resuscitation culture periods and routine morphological monitoring to ensure phenotypic stability.

### RNA extraction and quantitative real-time PCR(qRT-PCR)

Total RNA was extracted from NB cells using TRIzol™ reagent(Ambion, USA), followed by cDNA synthesis with HiScript® II Q RT SuperMix(Vazyme, China) according to the manufacturer's specifications. qRT-PCR analysis was performed on a LightCycler® 96 system(Roche, Switzerland) using AceQ® qPCR SYBR Green Master Mix(Vazyme, China), with thermal cycling parameters set as follows: initial denaturation at 95 °C for 5 min, 40 cycles of denaturation at 95 °C for 10 s, annealing at 60 °C for 30 s, and extension at 72 °C for 30 s, concluding with melt curve analysis(95 °C for 15 s, 60 °C for 60 s, 95 °C for 15 s).  $\beta$ -actin mRNA expression was used for normalization based on its constitutive expression across cell lineages. Relative quantification was determined through the  $2^{-\Delta\Delta C_t}$  method, with all primer sequences(General Biosystems, China) provided in Table S1.

### Establishment of stable and transient transfection models

Lentiviral vectors expressing *HIST1H1B*-specific shRNA(GeneChem, China) were constructed to knock-down target gene expression, with a non-targeting GFP-expressing scramble vector serving as the negative control. Following transduction, stable polyclonal populations were selected using 1  $\mu$ g/mL puromycin(Merck, Germany) for 72 h, with transfection efficiency confirmed by fluorescence microscopy. All shRNA sequences were documented in Table S2.

### Cell proliferation assay

A total of  $5 \times 10^3$  cells were seeded into each well of 96-well plates, with each well containing 100  $\mu$ L of culture medium. At specific time points on 24, 48, 72 and 96 h, 10  $\mu$ L of CCK-8 solution(APEX-BIO, USA) and 90  $\mu$ L of fresh culture medium were added to each well. Two hours after the addition, the optical density was measured at a wavelength of 450 nm.

### EdU assay

Cell proliferation activity was assessed using the Cell-Light™ EdU Apollo 567 In Vitro Kit(RiboBio, China) with optimized protocols. Briefly,  $5 \times 10^4$  cells/well were seeded in 24-well plates and synchronized in serum-free medium for 12 h prior to EdU pulse-labeling. Cells were incubated with 50  $\mu$ M EdU reagent(1:1000 dilution in complete medium) for 2 h at 37 °C with 5% CO<sub>2</sub>, followed by fixation with 4% paraformaldehyde and permeabilization using 0.5% Triton X-100. Subsequent fluorescent staining was performed sequentially with Apollo® 567 and Hoechst 33,342 nuclear counterstain, according to manufacturer's specifications.

### Transwell assay

The migratory and invasive capacities of tumor cells were assessed using Transwell chambers(8- $\mu$ m pore polycarbonate membrane). For invasion assays, the upper chambers were pre-coated with 50  $\mu$ L Matrigel basement membrane matrix(Corning, USA) and allowed to polymerize for 1 h at 37 °C. The lower chambers were filled with 750  $\mu$ L DMEM supplemented with 10% fetal bovine serum as a chemoattractant. Transfected cells( $1 \times 10^5$  cells/well) suspended in 200  $\mu$ L serum-free DMEM were seeded into the upper chambers. Following 48 h incubation at 37 °C with 5% CO<sub>2</sub>, non-migratory cells on the upper membrane surface were removed by cotton swab abrasion. Cells that traversed the membrane were fixed with 4% paraformaldehyde, stained with 0.5% crystal violet, and thoroughly washed with PBS.

## Results

### Preparation of NB chip data, compilation of clinical information, and data integration

First, we illustrated the specific procedure of this study through Fig. 1. In order to obtain a chip matrix data with a large sample size, we initially selected the GSE49710 and E-MTAB-8248 cohorts from the GEO and Array-Express databases, which contain 498 and 223 clinical samples respectively. The data was transformed using Log<sub>2</sub> conversion, resulting in a final chip matrix dataset comprising 721 NB samples. Additionally, the cohort comprising 154 NB patients from the TARGET database and the GSE16476 cohort from GEO, which included 88 NB patients, were used to validate the accuracy of the constructed model. The GSE89413 cohort contained chip data from 39 NB cell lines and was utilized for analyzing the ER stress related risk score of each NB cell line. The detailed information of all cohorts was shown in Table 1.

### Consensus clustering analysis for ERSRGs

We obtained ERSRGs from the Human Gene Set "Set-GOBP\_RESPONSE\_TO\_ENDOPLASMIC\_RETICULUM\_STRESS" in the MSigDB database, which included 258 genes. Then, we intersected these 258 genes with all genes in the merged matrix, resulting in 250 ERSRGs for further analysis. By setting the criteria of HR  $\neq$  1 and  $p < 0.05$ , we conducted a univariate cox regression analysis of the 250 ERSRGs with the prognosis of the patients, and obtained 173 ERSRGs that are closely related to the prognosis of NB. The top 10 ERSRGs with the most significant statistical differences were *TMEM33*( $p = 1.65E-34$ ), *DNAJB2*( $p = 6.34E-29$ ), *AIFM1*( $p = 1.43E-27$ ), *UGCG1*( $p = 2.08E-26$ ), *UBE4B*( $p = 2.19E-23$ ), *TP53*( $p = 3.27E-23$ ), *ELAVL4*( $p = 6.24E-23$ ), *PIK3R1*( $p = 7.45E-22$ ), *EIF2S1*



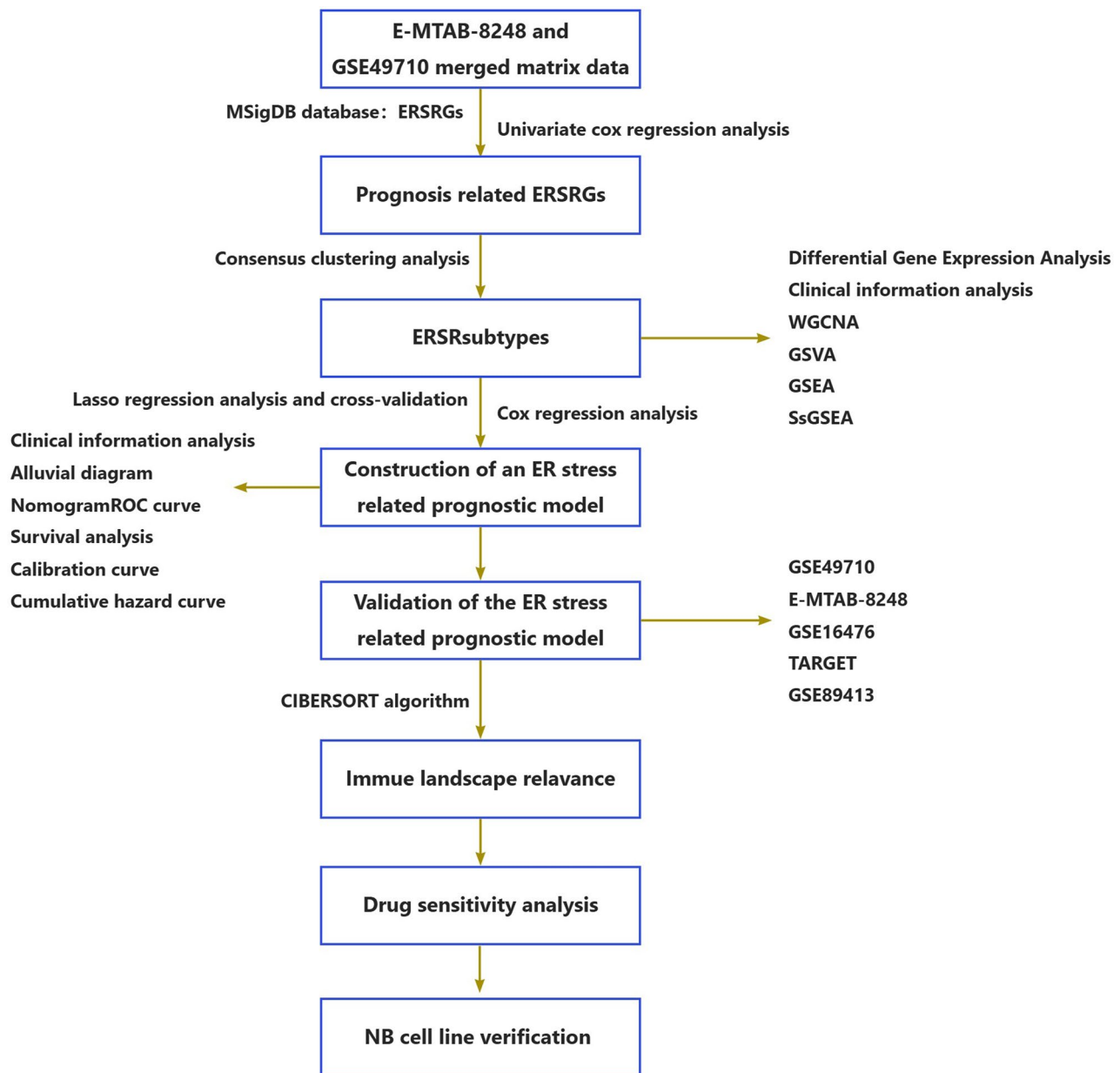


**Fig. 1** The flowchart of this study

( $p = 8.57 \times 10^{-22}$ ), and *PPP1R15B* ( $p = 1.43 \times 10^{-21}$ ). The 10 ESRGs most closely related to the prognosis of NB were *OPA1* (HR = 5.59), *C11orf10* (HR = 5.56), *AIFM1* (HR = 5.45), *EIF2S1* (HR = 5.22), *TOR1A* (HR = 5.07), *TMEM33* (HR = 4.95), *UBA5* (HR = 4.89), *DNAJB2* (HR = 0.21), *TMCO1* (HR = 4.50), and *ATF6* (HR = 4.39). The 53 ESRGs with the most significant statistical differences were displayed in a forest plot (Fig. 2A, Additional file 1). By conducting consensus clustering analysis, we determined that setting the number of clusters ( $k$ ) to 2 resulted in the most significant decrease in the slope of the cumulative distribution function (CDF), indicating the optimal clustering effect (Fig. 2B-C). PCA showed that the 721 NB samples could be ideally clustered

into two distinct subtypes (Fig. 2D). Further KM survival analysis showed significant differences in prognosis between the two subtypes, with poorer prognosis in cluster B (Fig. 2E). Given that the two subtypes hold clinical significance, we performed a differential gene analysis and uncovered 165 differentially expressed ESRGs between them. The top 10 genes with the largest expression differences were *PDIA2* ( $\text{Log}_2\text{FC} = -1.45$ ), *FBXO2* ( $\text{Log}_2\text{FC} = -1.22$ ), *TNFRSF10B* ( $\text{Log}_2\text{FC} = 1.17$ ), *MAGEA6* ( $\text{Log}_2\text{FC} = 1.12$ ), *MAP3K5* ( $\text{Log}_2\text{FC} = -1.11$ ), *TP53* ( $\text{Log}_2\text{FC} = 1.08$ ), *PIK3R1* ( $\text{Log}_2\text{FC} = -1.06$ ), *CLU* ( $\text{Log}_2\text{FC} = -0.92$ ), *IL8* ( $\text{Log}_2\text{FC} = 0.90$ ), and *FBXO44* ( $\text{Log}_2\text{FC} = -0.85$ ) (Additional file 2). We presented a box plot to illustrate the 29 ESRGs that

**Table 1** The detailed information of the public datasets in this research

Cohort	Database	Major clinical information							
		MYCN+/-	Age (months)		COG stage		INSS stage		
GSE49710	GEO	MYCN+	92	> 18	193	High	176	I	121
Platform: Agilent–020382 Human Custom Microarray 44k		MYCN-	401	≤ 18	305	Low	322	II	78
Country: China		Unknown	5					III	63
Cases: 498								IV	183
								IVs	53
E-MTAB-8248	Array-Express	MYCN+	47	> 18	119			I	29
Platform: Agilent–020382 Human Custom Microarray 44k		MYCN-	176	≤ 18	104			II	39
Country: Germany								III	36
Cases: 223								IV	89
								IVs	30
GSE16476	GEO	MYCN+	16	> 12	49			I	8
Platform: Affymetrix Human Genome U133 Plus 2.0 Array		MYCN-	72	≤ 12	39			II	15
Country: Netherlands								III	13
Cases: 88								IV	40
								IVs	12
TARGET	TARGET	MYCN+	33	> 18	125			I	0
Platform: Illumina Hiseq 2000		MYCN-	120	≤ 18	29			II	1
Organization: COG		Unknown	1					III	6
Cases: 154								IV	126
								IVs	21
GSE89413	GEO								
Platform: Illumina NextSeq 500									
Country: America									
NB cell number: 39									

displayed the most significant statistical differences (Fig. 2F). Further statistical analysis to delineate the clinical disparities between the two ERSRsubtypes revealed that the high-risk ER stress related cluster(ERSRcluster) B, associated with poorer prognosis, was significantly correlated with established adverse prognostic factors—including age>18 months, MYCN amplification, advanced INSS stage(III-IV), and high COG risk—compared to the more favorable ERSRcluster A(all  $p < 0.001$ ) (Fig. 2G, Figure S1). These findings demonstrated that the consensus clustering analysis employed in this study successfully categorized the 721 NB patients and revealed two distinct ERSRsubtypes with divergent prognoses. The ERSRcluster associated with poorer prognosis showed significant correlations with several clinical features indicative of worse outcomes. Consequently, exploring the differences in the pathogenesis between the two subtypes provides new insights for the treatment of NB.

**Analyses of GSEA, GSVA and immune cell infiltration between different ERSRsubtypes**

The results of GSEA based on “c5.go.v7.4.symbols.gmt” indicated that the five most significant pathways with the most distinct differences were: “GOBP\_NUCLEAR\_CHROMOSOME\_SEGREGATION”, “GOBP\_CHROMOSOME\_SEGREGATION”, “GOBP\_DNA\_DEPENDENT\_

DNA\_REPLICATION”, “GOBP\_MITOTIC\_SISTER\_CHROMATID\_SEGREGATION”, and “GOBP\_MEIOTIC\_CHROMOSOME\_SEGREGATION” (Fig. 3A). The five most prominent pathways based on “c5.go.v7.4.symbols.gmt” were: “KEGG\_CELL\_ADHESION\_MOLECULES\_CAMS”, “KEGG\_CELL\_CYCLE”, “KEGG\_HEMATOPOIETIC\_CELL\_LINEAGE”, “KEGG\_AXON\_GUIDANCE”, and “KEGG\_DNA\_REPLICATION” (Fig. 3B). We further conducted GSVA analysis on the two subtypes. Based on “c5.go.v7.4.symbols.gmt”, the five pathways with the most significant expression differences were: “GOCC\_METHYLOSOME”, “GOCC\_SMN\_SM\_PROTEIN\_COMPLEX”, “GOBP\_NUCLEOBASE\_BIOSYNTHETIC\_PROCESS”, “GOBP\_SNO\_S\_RNA\_METABOLIC\_PROCESS”, and “GOBP\_SNO\_S\_RNA\_PROCESSING” (Fig. 3C). According to “c2.cp.kegg.v7.4.symbols.gmt”, the five most significant pathways with differences were: “KEGG\_BASE\_EXCISION\_REPAIR”, “KEGG\_NUCLEOTIDE\_EXCISION\_REPAIR”, “KEGG\_DNA\_REPLICATION”, “KEGG\_CYSTEINE\_AND\_METHIONINE\_METABOLISM”, and “KEGG\_PYRIMIDINE\_METABOLISM” (Fig. 3D). Previous studies had shown that ER stress was closely related to the TME. We performed immune cell infiltration analysis on two different ER subtypes using SsGSEA, and the results suggested that there were significant differences in the distribution of 18 types of

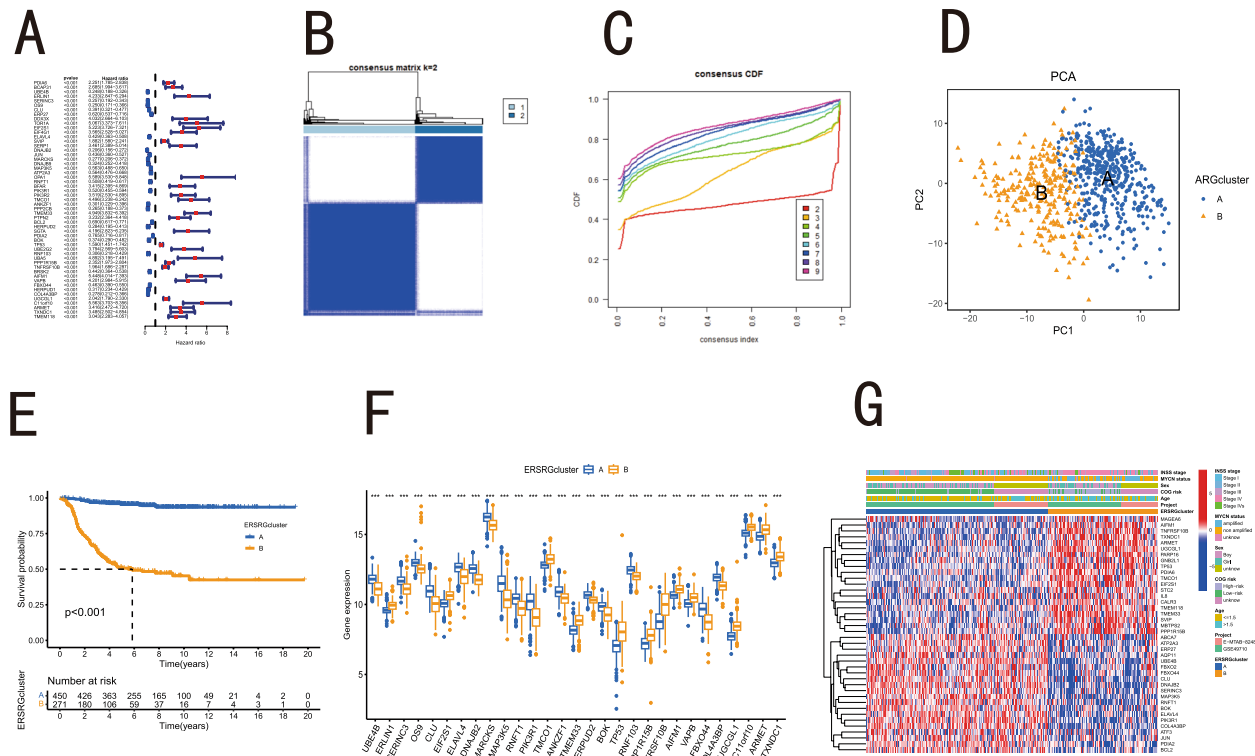


**Fig. 2** Acquisition of ERSRsubtypes in NB. **A** The forest plot presents 53 ESRGs that are most closely associated with the prognosis of NB through univariate cox regression analysis. **B-C** Consistency clustering analysis suggested that all the samples could be effectively clustered into 2 clusters ( $k=2$ ). **D** All samples could be ideally clustered into 2 distinct subtypes through PCA. **E** KM survival analysis showed significant differences in prognosis between two ER stress related subtypes ( $p < 0.001$ ). **F** The box plot presented the 29 ESRGs with the most significant statistical differences in expression between two clusters. **G** The heatmap showed the distribution of various clinical characteristics and presented part of the ESRGs with the most statistically significant differences in expression in two clusters. All the samples with *MYCN* amplification were included in the ERSRcluster B. \*\*\*,  $p < 0.001$ . ER, endoplasmic reticulum; NB, Neuroblastoma; PCA, principal component analysis; KM, kaplan-meier; ERSRGs, ER stress related genes; ERSRcluster, ER stress related cluster; ERSRsubtype, ER stress related subtype

immune cells between the two subtypes. In addition to an increased distribution of Activated.CD4.T.cell and Type.2.T.helper.cell in the poor prognostic ERSRsubtype B, the distribution of the other 16 types of immune cells was reduced in this subtype (Fig. 3E). The above results indicated that there were many differentially expressed signaling pathways in the two different prognostic subtypes and these pathways might directly or indirectly participate in the regulatory role of ER stress in the occurrence and development of NB.

#### Identifying hub genes between different subtypes through WGCNA

According to WGCNA, we first removed outlier samples and genes, and then performed clustering analysis on the remaining samples (Fig. 4A). By setting a threshold of 7 and  $R^2=0.92$ , we were able to construct an ideal scale-free network and cluster it into 18 modules (Fig. 4B-C). These 18 modules were further merged into 14 modules by setting a height threshold of 0.25 (Fig. 4C-D). Among these 14 merged modules, 13 modules showed significant correlation with ER stress (Fig. 4E). Specifically,

MEgreen, MEtan, MEsalmon, MEgreenyellow, METurquoise, MEblue, and MEmagenta modules were negatively correlated with ER stress, while MELightcyan, MEcyan, MEblack, MEpink, MEyellow, and MEgrey modules were positively correlated with ER stress. Among all the modules, the METurquoise module showed the strongest correlation with ER stress in NB, with a correlation index of 0.8 (Fig. 4E). We further screened 93 core genes from the METurquoise module with  $GS > 0.5$  and  $MM > 0.8$  (Fig. 4F, Additional file 3), and intersected them with 58 DEGs ( $|\log_2 FC| > 2$  and  $p < 0.05$ ) between two subtypes (Additional file 4). Finally, we identified 4 hub genes that played a crucial role in ERSRsubtypes: *NTRK1*, *PTPRH*, *ZNF695*, and *HIST1H1B* (Fig. 4G). Based on these results, we found that ER stress plays an important role in the development of NB, and the hub genes identified in this study are involved in the regulation of ER stress in NB.

#### Construction of an ER stress related prognostic model

We randomly divided 721 pediatric cases into training and test groups, from which 17 key genes were

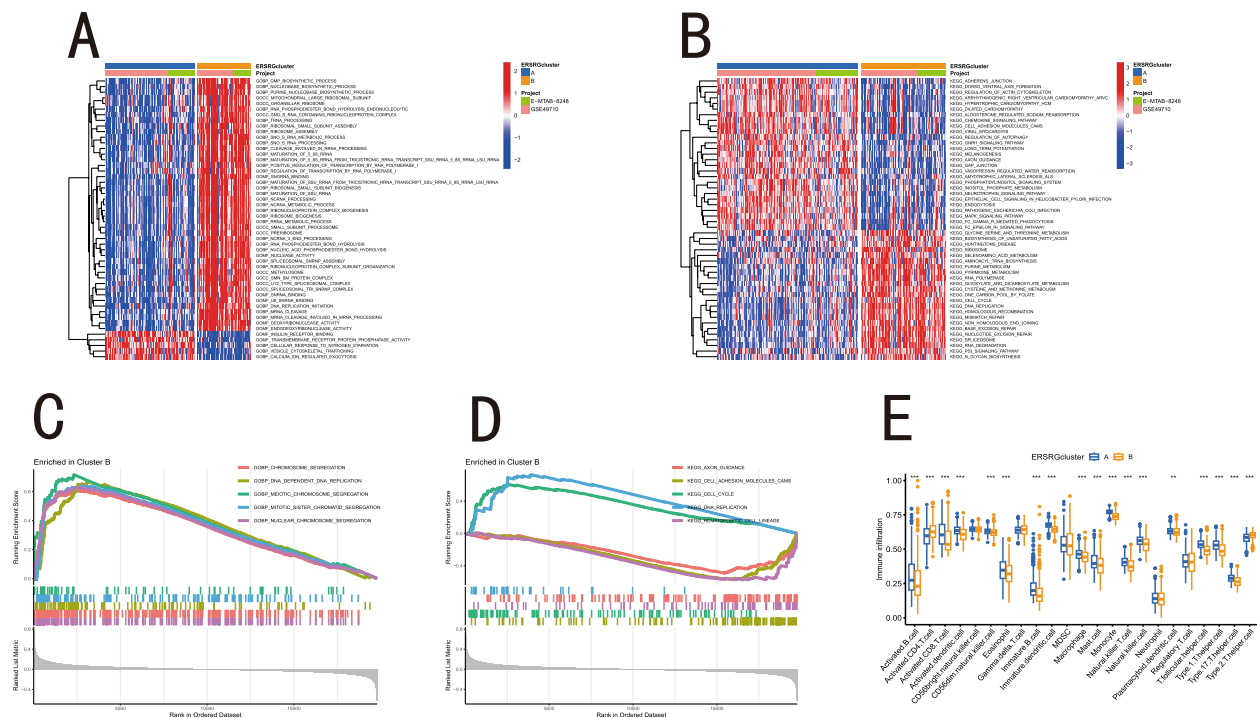


**Fig. 3** GSVA, GSEA, and immune cell infiltration analysis between two ERSRGclusters. **A-B** Enrich the differentially expressed pathways between the two clusters through GSVA. **C-D** Enrich the differentially expressed pathways between the two clusters through GSEA. **E** Conduct an analysis of the infiltration levels of 23 immune cells in the two clusters through SsGSEA. \*\*,  $p < 0.01$ ; \*\*\*,  $p < 0.001$ . GSVA, gene set variation analysis; GSEA, gene set enrichment analysis; ERSRGcluster, ER stress related cluster; SsGSEA, single-sample gene set enrichment analysis

identified through LASSO regression analysis and cross-validation (Fig. 5A), and 10 ERSRGs involved in model construction were determined by cox regression analysis, with detailed presentation of the full names of *ELAVL4*, *FBXO*, *MAP3K5*, *DNAJC10*, *ANKZF1*, *PPP2CB*, *TMEM33*, *SGTA*, *THBS4*, *UBE4A*, their weights in the predictive model (Table 2), and their specific locations on the chromosomes (Fig. 5B). Based on the predictive model, we conducted a risk assessment for each NB, and evenly categorized all samples into the high-risk or low-risk group. The results indicated that the expression of the 10 ERSRGs involved in the model construction was significantly different between the high-risk and low-risk groups (Fig. 5C, Additional file 5), with the risk scores of children in the ERSRGcluster B generally higher than those in the ERSRGcluster A (Fig. 5D). From the Alluvial diagram, we found that the majority of children in the ERSRGcluster A had lower risk scores, while almost all children in the ERSRGcluster B had high risk scores, and almost all surviving patients came from the low-risk group (Fig. 5E). The distribution of expression levels of differential genes, clinical traits such as age  $\geq 18$  months, *MYCN* amplified, high COG risk, and INSS stage III-IV were consistent across different risk groups and different clustering groups (Fig. 5F, Figure S1). Through the nomogram, we also found that the risk score could serve as an independent predictive factor for the prognosis of NB

patients, compared to other clinical indicators (Fig. 5G). The prognostic model demonstrated high predictive accuracy, as evidenced by the 1-, 3-, and 5-year area under the curve (AUC) values of 0.885, 0.878, and 0.898 in the total cohort; 0.923, 0.919, and 0.925 in the training set; and 0.844, 0.840, and 0.866 in the test set (Fig. 6A-C). The results of KM survival analysis and the ROC curve indicated that the predictive model could effectively predict the survival status of children in the total sample, training group, and test group (Fig. 6D-F). The calibration curve results showed that the model's predictions of 1-year, 3-year, and 5-year survival probabilities were close to the actual survival probabilities (Fig. 6G). Finally, through the cumulative hazard curve, we found that with the extension of follow-up time, the cumulative survival risk of patients in the high-risk group increased significantly, while the survival risk of the low-risk group changed slightly (Fig. 6H). These results demonstrated that our ER stress related prognostic model accurately predicted outcomes in NB patients, thereby establishing a foundation for its further validation across multiple independent datasets.

#### Validation of model accuracy across multiple datasets

In order to further validate the applicability of the ER stress related predictive model in other datasets, we performed additional analyses on GSE49710, GSE16476,



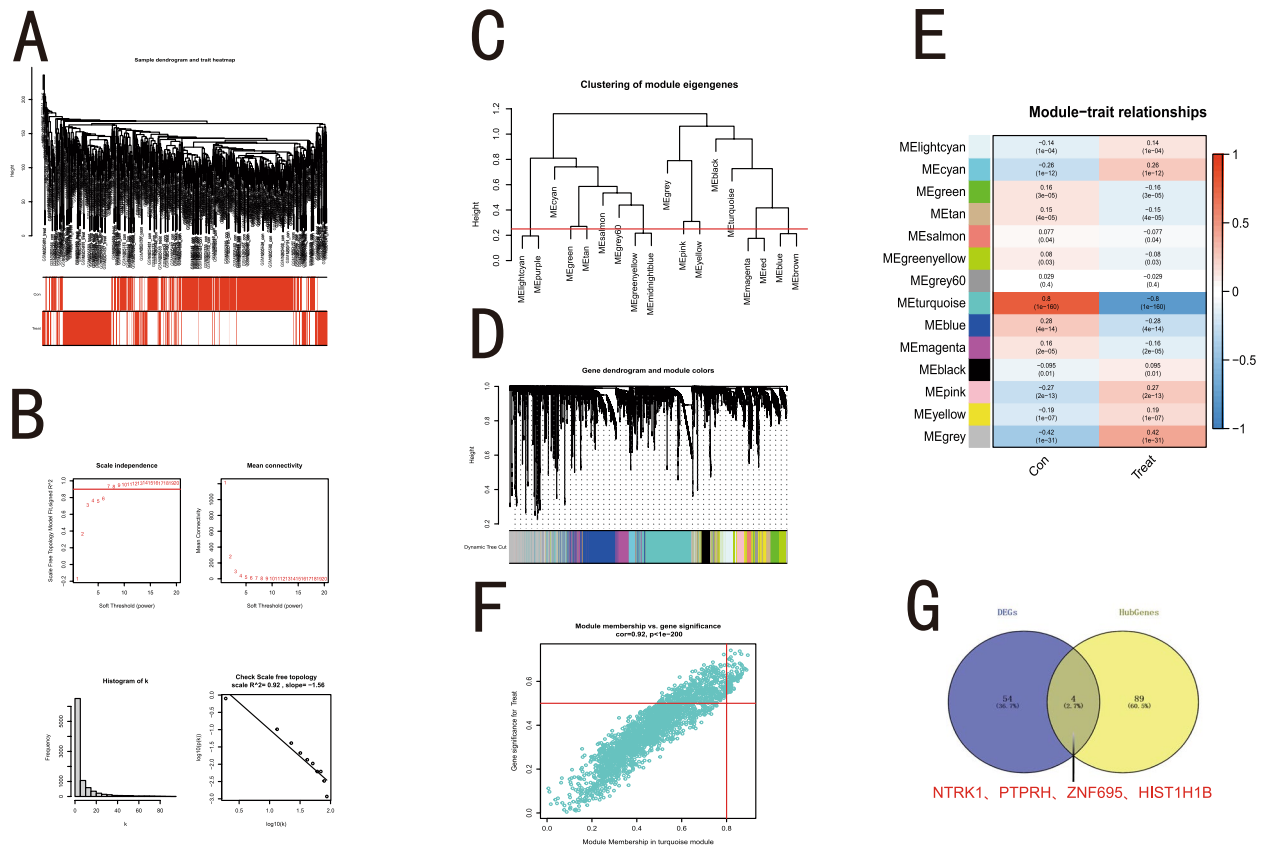


**Fig. 4** Identifying hubgenes between different ERSRsubtypes through WGCNA. **A** Clustering dendrogram of 721 samples. **B** By setting the threshold to 7 and with  $R^2$  equal to 0.92, we successfully constructed an ideal scale-free network. **C-D** All genes were included in 18 modules based on WGCNA. The 18 modules were further merged into 14 modules by further setting the standard with a height threshold of 0.25 (red line). **E** The heatmap of the correlation between the 14 modules and ER stress, among which the MEturquoise module has the strongest correlation with ER stress. **F** 93 core genes from the MEturquoise module were screened by setting the criteria of  $GS > 0.5$  and  $MM > 0.8$ . **G** A total of 4 hub genes were obtained based on the intersection of the core genes in the MEturquoise module and the DEGs between two ERSRGclusters. WGCNA, weighted gene co-expression network analysis; DEGs, differentially expressed genes; ER, endoplasmic reticulum; GS, gene significance; MM, module membership; DEGs, differentially expressed genes; ERSRGcluster, ER stress related cluster

E-MTAB-8248, and the TARGET cohorts. Based on the predictive formula, we first scored the samples from GSE49710 and E-MTAB-8248, which had a large sample size and comprehensive clinical data, and divided them into high-risk and low-risk groups. We found that the expression levels of the majority of the previously obtained ERSRGs that were differentially expressed were also different between high and low-risk groups of GSE49710 and E-MTAB-8248 (Fig. 7A-B). Moreover, clinical characteristics associated with poor prognosis, such as age  $\geq 18$  months, MYCN amplification, high COG risk, and INSS stage III-IV, were mainly concentrated in the high-risk group (Fig. 7A-B). In GSE49710 and E-MTAB-8248 cohorts, the risk score served as an independent prognostic indicator for NB patients (Fig. 7C-D). By grouping GSE49710, E-MTAB-8248, TARGET and GSE16476 cohorts, we observed that the high-risk group had significantly worse prognosis than the low-risk group in all four datasets (Fig. 7E-H). Utilizing this predictive

model, we analyzed the chip data of 39 NB cell lines from the GSE89413 cohort. The results showed that NGP, RD, CHP-212, SK-N-AS, COG-N-519, NB-69, LA-N-6, KELLY, COG-N-440, and NMB were the top ten cell lines with the highest risk scores, while SK-N-BE(2), COG-N-549, SK-N-BE(2)-C, NB-1691, SMS-SAN, COG-N-496, LA-N-5, NB-1643, NB-1, and Felix were the ten cell lines with the lowest risk scores (Fig. 7I). These findings demonstrated that the ER stress related prognostic model was applicable in various NB cohorts and could serve as an independent predictive indicator for prognosis. Furthermore, there were ER stress related cell subtypes in NB cell lines, providing a foundation for further cellular validation and mechanistic research.

#### Differences in immune cell infiltration between different risk groups of NB

Previous studies have shown that ER stress is closely related to the TME, and changes in the TME are closely

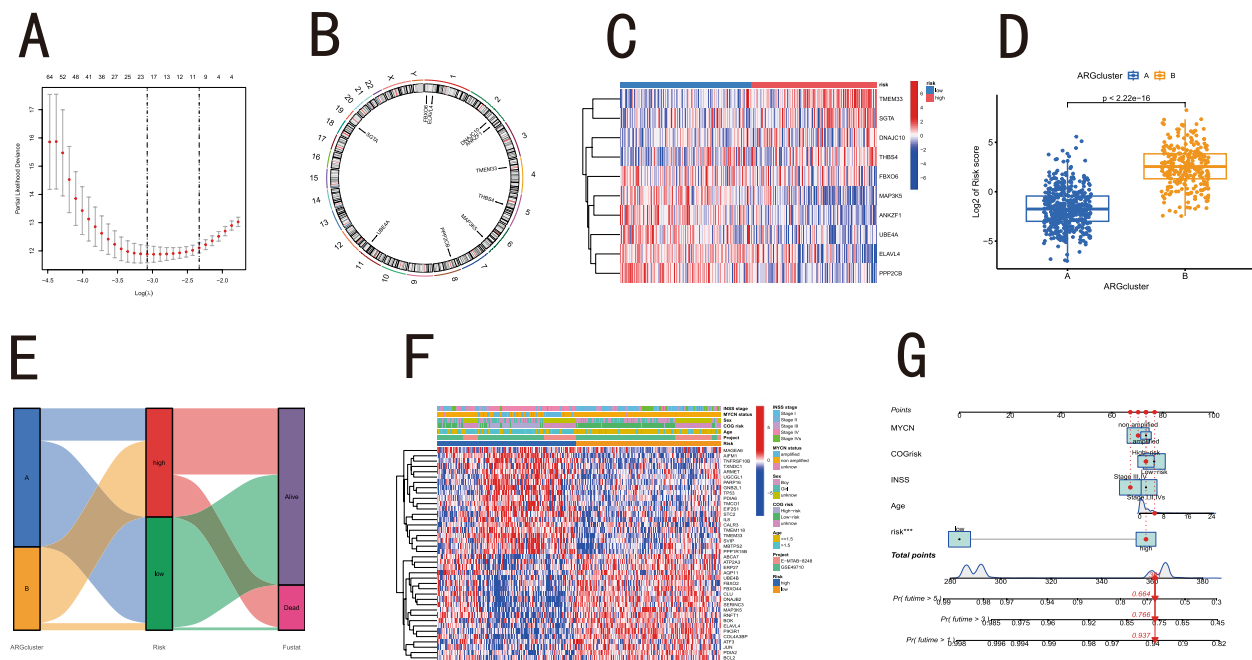


**Fig. 5** Construction of an ER stress related prognostic model. **A** We first determined these 17 key genes through Lasso regression analysis and cross validation. **B** The locations of 10 ERSRGs involved in model construction in the chromosome. **C** This heatmap showed the expression of the 10 ERSRGs involved in model construction in two different risk groups. **D** Based on the scoring formula, we calculated the risk scores of the 721 samples and grouped all the cases. **E** Alluvial diagram showed the grouping and living status of all the cases. **F** The heatmap showed the distribution of the clinical traits closely related to the prognosis and the differences in the expression of some ERSRGs in different risk groups. **G** Nomogram showed that the risk score could serve as an independent predictive factor for the prognosis of NB patients. ER, endoplasmic reticulum; LASSO, least absolute shrinkage and selection operator; ERSRGs, ER stress related genes; NB, Neuroblastoma

associated with tumor development, metastasis, and other characteristics [28–30]. Therefore, it is of great significance to explore the differences in immune cell infiltration between two ERSRsubtypes in studying the impact of ER stress on NB. Using the CIBERSORT algorithm, we scored the immune cells for each clinical sample and found significant differences in the distribution of eight immune cells between different risk groups. B cells memory, Plasma cells, T cells CD4 naive, and Neutrophils were more abundant in the high-risk group, while T cells CD4 memory resting, Monocytes, Macrophages M2, and Mast cells activated were highly expressed in the low-risk group (Fig. 8A). Heatmap also revealed significant correlations in the distribution levels between certain immune cell types in NB, especially positive correlations between T cells CD8, T cells regulatory, T cells CD4 naive, B cells naive, and T cells follicular helper, as well as negative correlations between distribution levels of the cell types mentioned above, Macrophages M0, Macrophages M2, and Mast cells activated. Among all the cell types, the strongest positive correlations were observed between T cells follicular helper and B cells naive (correlation index = 0.36), and between T cells CD8 and T cells regulatory (correlation index = 0.36). The strongest negative correlation was observed between B cells naive and Macrophages M0 (correlation index = -0.5) (Fig. 8B).

Using the estimation of stromal and immune cells in alignant tumour expression (ESTIMATE) algorithm, we found that although there were no differences in Stromal Score among different risk groups, the Immune Score and ESTIMATE Score were lower in the high-risk group (Fig. 8C), indicating a higher tumor cell purity and lower proportion of immune cells in this group. Analyses of the expression levels of the 10 genes involved in model construction and their relationship with the distribution levels of immune cells revealed significant correlations between these genes and various immune cell types, particularly *ELAVL4*, *FBXO6*, *PPP2CB*, and *TMEM33* (Fig. 8D). Finally, we performed a correlation analysis between risk scores and the distribution levels of all immune cells, and found a significant positive correlation between risk scores and the distribution levels of plasma cells and B cells memory, and a significant negative correlation between risk scores and the levels of T cells CD8 and T cells CD4 memory resting (Fig. 8E–H). These results indicated that there were significant differences in the distribution of immune cells between different NB subtypes associated with ER stress. Not only were there correlations among the distribution levels of immune cell types, but there were also connections between the expression levels of genes involved in model construction, patient risk scores, and the distribution levels of various immune

**Table 2** The detailed information of 10 ERSRGs involved in model construction

Gene name	Official full name	Ensemble id	Weight
ELAVL4	Embryonic Lethal, Abnormal Vision, Drosophila-Like 4	ENSG00000162374	-0.53335966415539
FBXO	F-Box Only Protein 41	ENSG00000163013	-0.524410927840551
MAP3K5	Mitogen-Activated Protein Kinase Kinase 5	ENSG00000197442	-0.287828908522957
DNAJC10	DnaJ Heat Shock Protein Family (Hsp40) Member C10	ENSG00000077232	1.59066427443646
ANKZF1	Ankyrin Repeat And Zinc Finger Peptidyl TRNA Hydrolase 1	ENSG00000163516	-1.0100276576851
PPP2CB	Protein Phosphatase 2 Catalytic Subunit Beta	ENSG00000104695	-1.05185809170224
TMEM33	Transmembrane Protein 33	ENSG00000109133	0.94596610343543
SGTA	Small Glutamine Rich Tetratricopeptide Repeat Co-Chaperone Alpha	ENSG00000104969	1.15422196718206
THBS4	Thrombospondin 4	ENSG00000113296	0.124547489619208
UBE4A	Ubiquitination Factor E4A	ENSG00000110344	-1.31873436820272

cell types. The infiltration of these immune cells might be closely related to ER stress in NB and have a significant impact on the TME, ultimately affecting the prognosis of NB patients.

**Chemotherapeutic response analysis between different ERSRsubtypes**

Currently, the treatment of NB remains a clinical challenge, and even with a combination of multiple

treatment modalities, the prognosis for high-risk NB patients remain poor [5–15]. Based on the predictive model constructed in this study, which is related to ER stress, we found that NB patients with poor prognostic factors such as age  $\geq 18$  months, *MYCN* amplification, high COG risk, and INSS stage III-IV were more likely to be included in the high-risk group. Therefore, we can have a better basis for selecting chemotherapy drugs that are more effective for the poor prognostic ERSRsubtype, and improve the prognosis of these NB patients by predicting the chemotherapy drug sensitivity of the two subtypes. The predictive results suggested that there were significant differences in the treatment efficacy of 149 chemotherapy drugs in the two different risk groups (Additional file 6, 7). We found a total of 18 chemotherapy drugs that showed better treatment efficacy in the high-risk group of NB(Additional file 6), and listed eight drugs with statistically significant differences in drug sensitivity (Fig. 9A). These results fully demonstrated that the 18 drugs we selected might have potential targeted effects on ER stress resistance in NB and would provide a basis for the clinical treatment of high-risk NB patients with the selected drugs.

***HIST1H1B* promoted the proliferation, migration and invasion of *MYCN*-amplified NB cells**

To further validate the accuracy of this study, we selected *HIST1H1B* among the 4 hub genes identified in two ERSRsubtypes. Previous studies have confirmed that all *MYCN*-amplified NB were classified into the ERSRsubtype with poor prognosis (Fig. 2G), and *HIST1H1B* was relatively up-regulated in *MYCN* amplified NB compared to non *MYCN* amplified NB(Additional file 4). We observed that the expression level of *HIST1H1B* was significantly elevated in *MYCN*-amplified NB cells (Fig. 10A). To further investigate the role of *HIST1H1B* in NB, we performed *HIST1H1B* knockdown in two *MYCN*-amplified cell lines: IMR-32 and SK-N-BE(2) (Fig. 10B-C). The results demonstrated that *HIST1H1B* knockdown significantly inhibited the proliferative capacity of both IMR-32 and SK-N-BE(2) cells (Fig. 10D-E). Additionally, the migration and invasion abilities of these tumor cells were markedly reduced (Fig. 10F-G). EdU assay further revealed that *HIST1H1B* knockdown exerted a pronounced inhibitory effect on the DNA replication process in SK-N-BE(2) (Fig. 10H). In conclusion, our findings indicated that *HIST1H1B* was highly expressed in *MYCN*-amplified NB cell lines and promoted the proliferation, migration, and invasion capabilities of *MYCN*-amplified NB cells, thereby further validating the accuracy of this research.

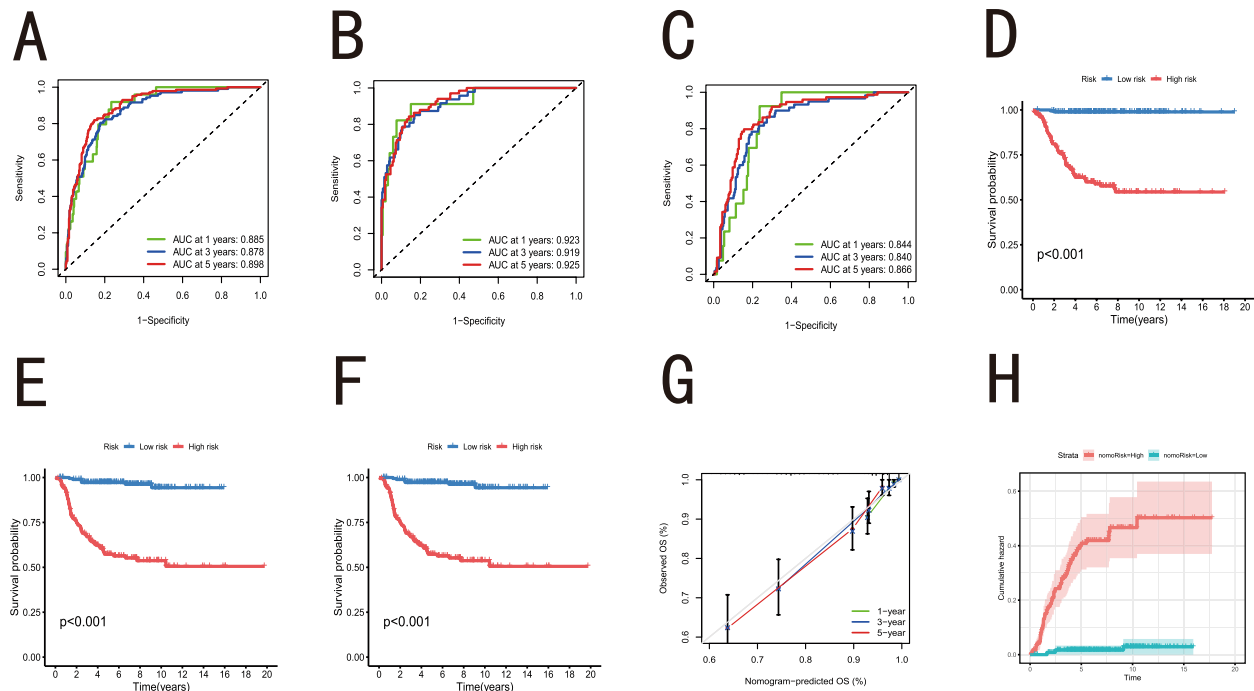


**Fig. 6** Verify the reliability of the ER stress related model through prognostic analysis. **A-C** The time-dependent AUC values of 1-year, 3-year, and 5-year survival rates in the total sample group, training group, and test group. **D-F** KM survival analysis indicated that the overall survival rate of the high-risk group children was significantly lower than that of the low-risk group children in the overall population, train group, and test group. **G** The cumulative hazard curve indicated that with the extension of follow-up time, the cumulative survival risk of the high-risk group was significantly higher than that of the low-risk group. **H** The survival calibration curve indicated that the prediction model constructed in this study had high accuracy in predicting the 1-year, 3-year, and 5-year overall survival rate of the children. ER, endoplasmic reticulum; AUC, area under the curve; KM, Kaplan-meier

## Discussion

NB is one of the most malignant solid tumors in children [1]. Currently, for high-risk NB, there are various clinical treatment options available. However, even with a combination of surgery, chemotherapy [6, 7], radiation [8, 9], autologous stem cell transplantation [10–12], and immunotherapy [12–15], the 5-year survival rate of patients is still low. Therefore, exploring the pathogenesis of high-risk NB and finding targeted drugs for NB will bring hope to these patients. In recent years, with the rapid development and popularization of gene chip technology and next-generation sequencing, analyzing the pathogenesis of diseases at the transcriptome level has become a reality, and its application in NB is particularly important. For example, N-myc functions as a crucial transcription factor that extensively regulates the transcription of key genes involved in tumor development in *MYCN* amplified NB [31–33]. This study was based on this technology to explore the mechanism of NB development. The ER is a central organelle involved in the synthesis, folding, and modification of secretory and transmembrane proteins [16]. Protein processing, modification, and folding in the ER are tightly regulated processes that determine cell function, fate, and survival [34]. Beyond its role in protein homeostasis, ER stress is increasingly recognized as a pivotal signaling hub that influences diverse cell fate

decisions, including proliferation, differentiation, and apoptosis, particularly in neural lineages [35]. In various cancers, the synergistic effects of different oncogenic, transcriptional, and metabolic abnormalities create unfavorable TME that disrupt the ER homeostasis of tumor cells and stromal cells, as well as infiltrating lymphocytes, leading to sustained ER stress [36–37]. Numerous studies have shown that this stress state controls various pro-tumor properties of cancer cells and dynamically reprograms the functions of innate immune cells and adaptive immune cells [17, 18, 38, 39]. Additionally, the abnormal activation of ER stress sensors and their downstream signaling pathways has become a key regulatory factor in tumor growth, metastasis, and response to chemotherapy, targeted therapy, and immunotherapy [34, 39, 40]. Currently, there is limited research on ER stress in NB. Therefore, based on chip data and clinical information of NB, this study explored the impact of ER stress mechanisms on the development of NB and changes in the TME. It also constructed a predictive model and predicted drug sensitivity related to ER stress.

In this study, we constructed a large sample cohort consisting of 721 cases, which would enhance the accuracy and generalizability of the results. Based on the expression levels of ESRGs, which were closely associated with the prognosis of NB patients, we successfully classified all



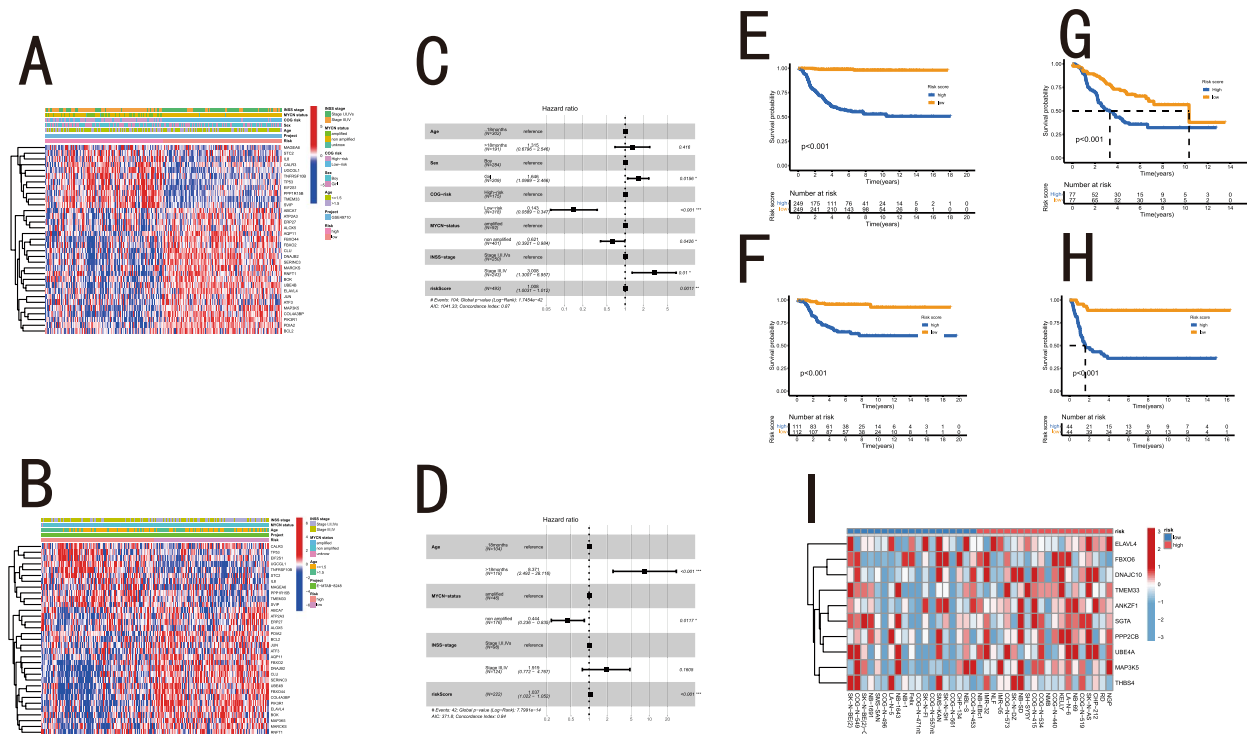


**Fig. 7** Verify the accuracy and general applicability of the model with multiple datasets. **A-B** The heatmap showed the distribution of the clinical traits closely related to the prognosis and the differences in the expression of some ERSRGs in different risk groups in GSE49710 and E-MTAB-8248. **C-D** Forest plots of multivariable cox regression analyses for the clinical features and risk scores derived from the ER stress related model in GSE49710 and E-MTAB-8248. **E-H** KM survival analysis indicated that the overall survival rate of the high-risk group children is significantly lower than that of the low-risk group children in GSE49710, E-MTAB-8248, GSE16476, and TARGET. **I** Risk assessment of NB cell lines in GSE89413 cohort based on the constructed model. \*,  $p < 0.05$ ; \*\*,  $p < 0.01$ ; \*\*\*,  $p < 0.001$ . ERSRGs, ER stress related genes; KM, kaplan-meier; TARGET, Therapeutically Applicable Research to Generate Effective Treatments; NB, Neuroblastoma

samples into two distinct ERSRsubtypes through consistent clustering analysis. Currently, numerous studies have shown the presence of ERSRsubtypes in adult malignant tumors such as lung cancer [41] and glioma [42], with significant differences in prognosis between the subtypes. The convergence between GSEA and GSVA results enhances confidence in our pathway findings, a strategy validated for profiling tumor dysregulation [43]. This study was the first to discover this phenomenon in NB, indicating the universality of ER stress in solid tumors and laying the foundation for investigating the roles of ER stress in the occurrence and development of NB.

We found a total of 173 ERSRGs associated with NB prognosis, including *PDIA2*, *FBXO2*, *TNFRSF10B*, *MAGEA6*, *MAP3K5*, *TP53*, *PIK3R1*, *CLU*, *IL8*, and *FBXO44*, which showed differential expression levels between different ERSRsubtypes. This result suggested that differentially expressed ERSRGs might be involved in the occurrence and development of NB through their participation in ER stress regulation. Previous studies have found high expression of *PDIA2* in colon cancer where it serves as a molecule linker between ER stress and metabolic reprogramming [44]. Parthenolide can inhibit the proliferation of lung cancer cells through the

ER stress pathway, and inhibition of *TNFRSF10B* can suppress parthenolide-induced apoptosis in lung cancer cells [45]. *MAP3K5*, as an important member of the *IRE1α*-*TRAF2*-*MAP3K5*-*JNK* axis, promotes NF- $\kappa$ B and AP1 activation to enhance inflammatory responses in cancer cells [46]. Previous studies have shown that *TP53*, as an important transcription factor, is upregulated under ER stress conditions and is involved in ER stress induced cell apoptosis [47], and NF- $\kappa$ B activation caused by ER stress is an important factor in increasing *TP53* expression [48]. Therefore, the above mentioned genes closely related to ER stress may play an important role in the occurrence and development of NB through the ER stress pathway. Further analysis revealed that some clinical features associated with prognosis, including age  $\geq 18$  months, *MYCN* amplification, high COG risk, and INSS stage III-IV, were significantly enriched in the poor prognostic ERSRsubtypes. Among these clinical features, *MYCN* amplification needs to be emphasized. Previous studies have shown that as an important member of the *MYC* protein family, N-myc shares many biological functions with *MYC* [31]. The *MYC* protein family can activate the UPR through various pathways. Firstly, the upregulation of overall transcription and translation induced

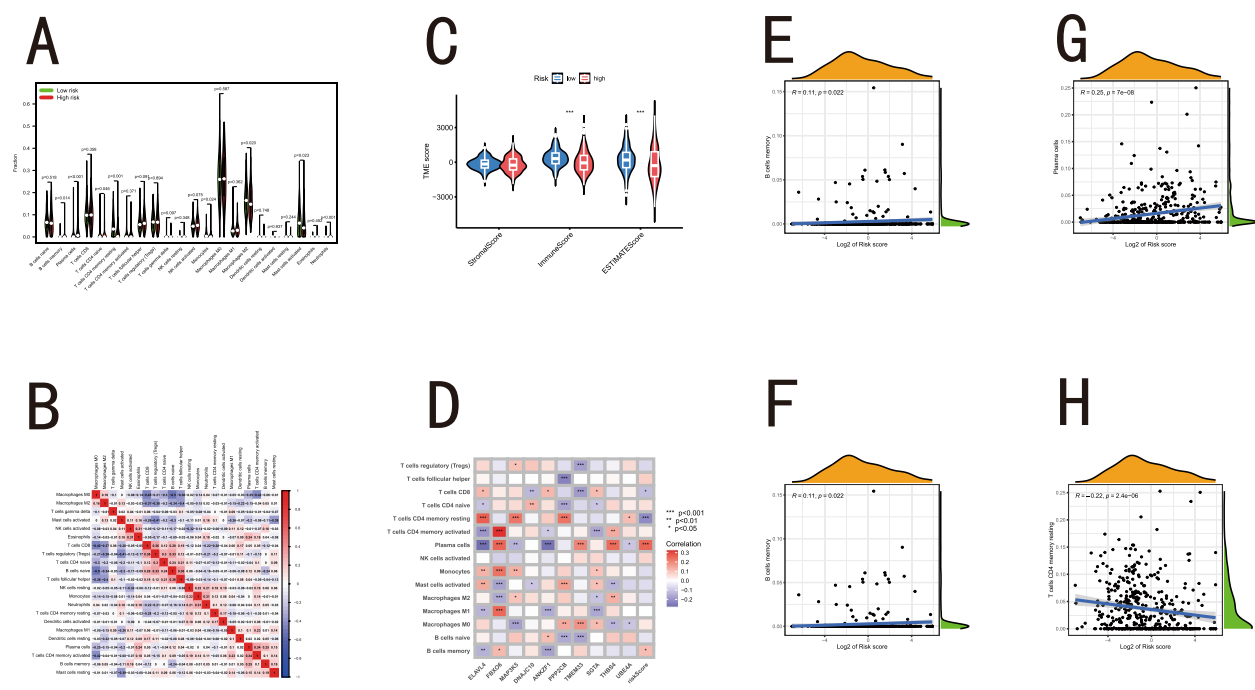


**Fig. 8** Analysis of immune cell infiltration in different risk groups. **A** Analysis of the differences in immune cell infiltration in different ER stress related risk groups based on the CIBERSORT algorithm. **B** The heatmap showing the correlations of infiltration levels among various immune cells. **C** Analysis of the disparities of the TME in two ER stress related risk groups. **D** The correlations between the infiltration levels of immune cells and the expression levels of the CIBERSORT 10 ERSRGs involved in model construction. **E-H** There is a significant correlation between risk scores and the levels of T cells CD8, B cells memory, plasma cells, and T cells CD4 memory resting. \*,  $p < 0.05$ ; \*\*,  $p < 0.01$ ; \*\*\*,  $p < 0.001$ . ER, endoplasmic reticulum; CIBERSORT, cell-type identification by estimating relative subsets of RNA transcripts; ERSRGs, ER stress related genes

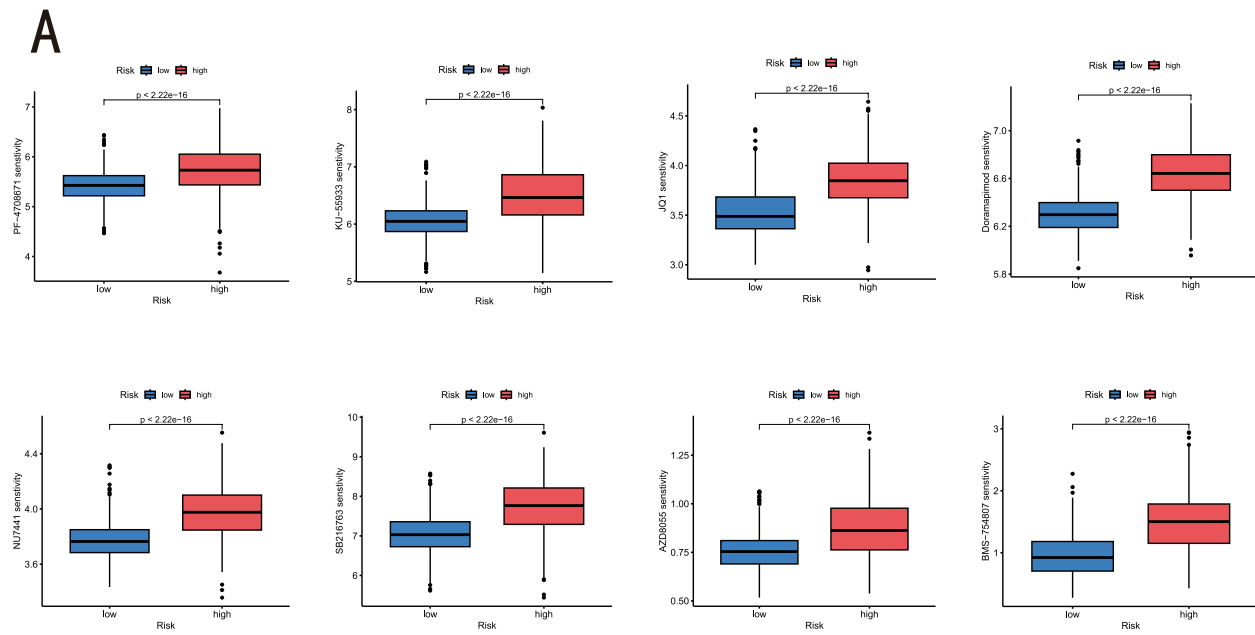


**Fig. 9** Chemotherapeutic response analysis between different ER stress related subtypes. **A** The eight kinds of drugs predicted to be the most sensitive to the high-risk group. ER, endoplasmic reticulum

by MYC increases the production of ribosomal proteins and protein load, thereby activating all branches of UPR [34, 49]. Secondly, MYC further binds to the promoter and enhancer regions of genes encoding IRE1α, positively regulating its transcription and increasing IRE1α protein levels [50]. Additionally, MYC can form heterodimers with XBP1s in the nucleus to regulate classical UPR genes and lipid metabolism genes [50]. MYC also interacts with

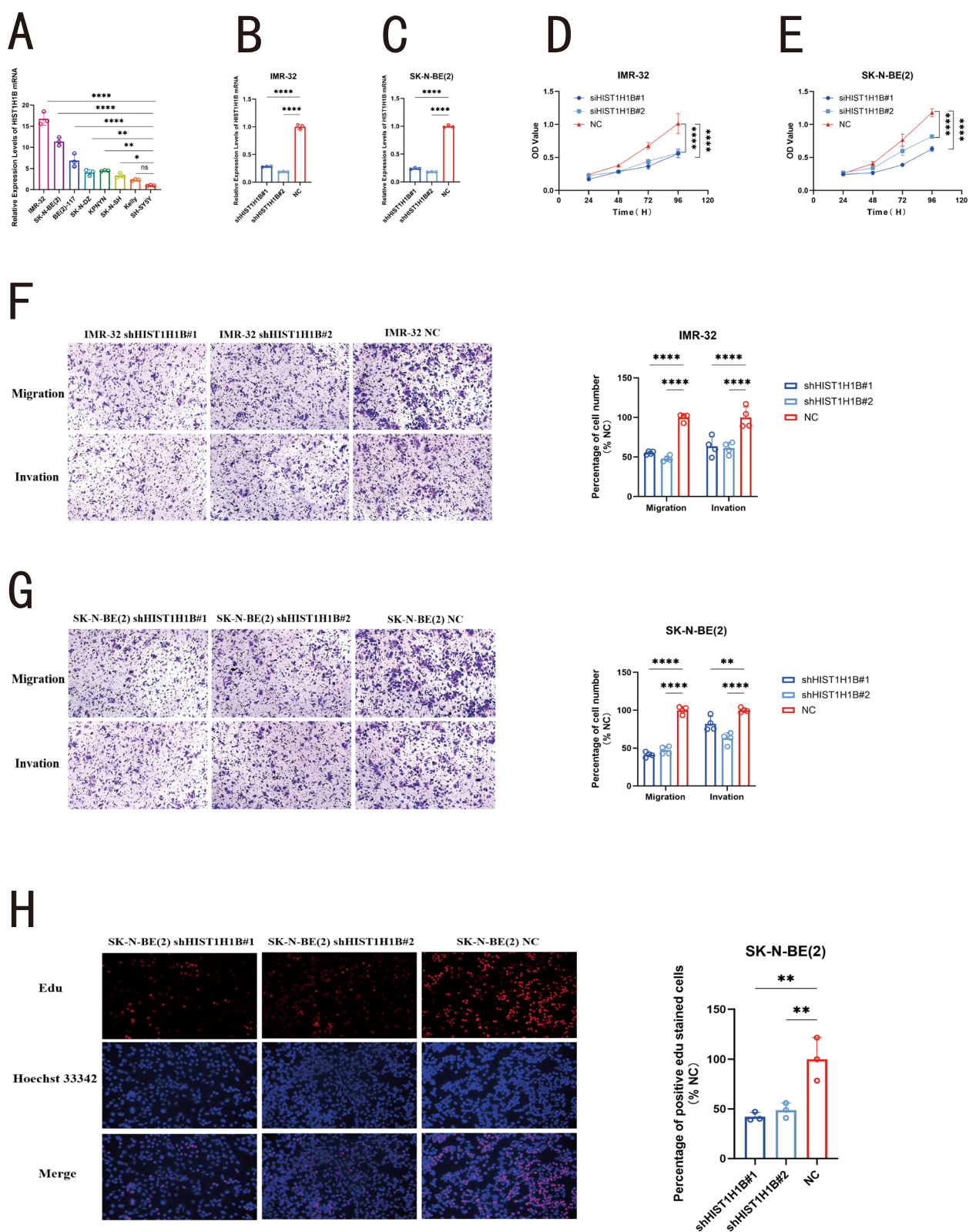


**Fig. 10** (See legend on next page.)

(See figure on previous page.)

**Fig. 10** *HIST1H1B* promoted the proliferation, migration and invasion of *MYCN*-amplified NB cells. **A** In addition to the *MYCN*-amplified NB cell line Kelly, the expression level of *HIST1H1B* in other *MYCN*-amplified NB cells, such as IMR-32, SK-N-BE(2), BE(2)-117, SK-N-DZ, and KPNYN, is significantly higher than that in the *MYCN* non-amplified NB cell lines SK-N-SH and SH-SY5Y. **B** We established *HIST1H1B*-knockdown IMR-32 cell lines via lentiviral transduction. **C** We established *HIST1H1B*-knockdown SK-N-BE(2) cell lines via lentiviral transduction. **D** The CCK8 assay indicated that knockdown of *HIST1H1B* could significantly inhibit the proliferative ability of IMR-32. **E** The CCK8 assay indicated that knockdown of *HIST1H1B* could significantly inhibit the proliferative ability of SK-N-BE(2). **F** The Transwell assay suggested that the knockdown of *HIST1H1B* could significantly inhibit the migration and invasion abilities of IMR-32 cells. **G** The Transwell assay suggested that the knockdown of *HIST1H1B* could significantly inhibit the migration and invasion abilities of SK-N-BE(2). **H** The EdU assay indicated that the knockdown of *HIST1H1B* significantly inhibited the DNA replication ability of SK-N-BE(2). \*,  $p < 0.05$ ; \*\*,  $p < 0.01$ ; \*\*\*,  $p < 0.001$ ; \*\*\*\*,  $p < 0.0001$ . NB, Neuroblastoma; CCK8, Cell Counting Kit-8; EdU, 5-Ethynyl-2'-deoxyuridine

ATF4 to regulate amino acid transporters, biosynthesis, antioxidant pathways, and autophagy. Finally, the MYC-ATF4 complex regulates eukaryotic translation initiation factor 4EBP1 to decrease translation and protein toxicity stress [51]. The diverse biological functions of the MYC family suggest that *MYCN* amplification can affect the occurrence and development of NB through the ER stress pathway, and *MYCN* amplified NB may promote tumor cell malignancy by adapting to ER stress.

WGCNA can cluster genes with similar expression patterns and analyze the correlation between modules and specific traits or phenotypes. It is widely used in the identification of candidate biomarkers or therapeutic targets and in the study of the association between phenotypic traits and genes [52]. To further investigate the key genes in the two ERSRsubtypes, we conducted WGCNA analysis and successfully obtained four key genes: *NTRK1*, *PTPRH*, *ZNF695*, and *HIST1H1B*. Jiao B used bioinformatics analysis to evaluate the transcriptional response of SH-SY5Y cells overexpressing *NTRK1* and found that upregulated genes were mainly enriched in response to ER stress and protein folding in the ER [53]. *PTPRH*, as an upstream gene of the PI3K/AKT/mTOR pathway, promotes the phosphorylation of PI3K/AKT/mTOR and facilitates the proliferation, migration, and invasion of non-small cell lung cancer [54]. The phosphorylation of the PI3K/AKT/mTOR pathway is an important pathway for SH-SY5Y cells to resist ER stress [55]. Currently, there is limited research on *ZNF695* and *HIST1H1B*, and further basic research is needed to confirm their roles in ER stress. Based on this current situation, we selected *HIST1H1B* as the focus of our further investigation. As a core member of the linker histones, *HIST1H1B* has been minimally studied in tumors, with no existing research reports specifically addressing its role in NB. Our findings demonstrated that *HIST1H1B* was consistently highly expressed in *MYCN*-amplified NB cells. Moreover, elevated *HIST1H1B* expression promoted tumor proliferation, migration, and invasion, which further validated the reliability of our research conclusions.

Using multivariable cox regression analysis, we have obtained an ideal prognostic prediction model for NB related to ER stress. This model accurately stratified NB patients into high and low-risk groups based on their prognoses. Furthermore, clinical characteristics

associated with poor prognosis, such as age  $\geq 18$  months, *MYCN* amplification, high COG risk, INSS stage III-IV, were also widely enriched in the poor prognostic subtype. Nomogram, calibration curves, cumulative risk curves, and decision curves all indicated that the predictive model we constructed could be used as an independent prognostic indicator for predicting the prognosis. The ability of our nomogram to provide independent prognostic value, validated across multiple metrics, finds support in similar robust predicting approaches [56]. In recent years, numerous studies have shown that constructing disease prediction models based on chip data and transcriptome data related to a specific biological feature, especially prognostic models for tumors, not only accurately predict disease progression in patients, but also have good guiding significance for basic research on the specific role of the biological feature in disease occurrence and development [41–42, 57]. We obtained a total of 10 ERSRGs: *ELAVL4*, *FBXO*, *MAP3K5(ASK1)*, *DNAJC10*, *ANKZF1*, *PPP2CB*, *TMEM33*, *SGTA*, *THBS4*, and *UBE4A* that participated in the construction of the model. All of these 10 genes were important genes involved in ER stress, and some of them had been directly or indirectly confirmed to be involved in the ER stress response in NB. It was found that significant IRE1/ASK1/JNK activation existed and was inhibited by salubrinal in SH-SY5Y cells treated with ceramide [58]. Thomas CG found that high expression of *DNAJC10* decreased the survival of SH-SY5Y by down-regulating the UPR, raising the possibility that *DNAJC10* could be a target for anti-NB approaches [59]. *UBE4A* has been found to be a protective gene that counteracts tumors through the ubiquitination pathway, and low expression of *UBE4A* is observed in NB with 11q deletion [60]. Studies have shown that *UBE4A* may work synergistically with its homolog *UBE4B* to exert anti-cancer effects, and the inactivation of either protein may promote the development of NB [60]. Whether they are involved in the occurrence and development of tumors through the ER stress pathway still requires further research.

Numerous studies have shown that the ER stress response in cancer cells can affect malignant progression by altering the function of coexisting immune cells in the TME [15, 16, 36–39]. Various situations in the TME help maintain the harmful ER stress response of



infiltrating immune cells [36–38]. The ER stress-linked TME remodeling we observed is mechanistically supported by recent studies on ER-targeted therapies in neural tumors [61]. Through model construction, we found that high risk scores were positively correlated with the expression levels of plasma cells and B cells memory, while negatively correlated with the expression levels of T cells CD8 and T cells CD4 memory resting in NB. B cells differentiate and enter peripheral immune organs after development in central immune organs, and differentiate into plasma cells and memory B cells under conditions of antigen stimulation. As part of immune-infiltrating B cells, both plasma cells and memory B cells can strongly affect patients' responses to anti-cancer chemotherapies and immunotherapies, as well as clinical outcomes in various cancers [62–64]. As the final form of B cells, antibody secretion by plasma cells triggers mechanisms such as antibody-dependent cell-mediated cytotoxicity and complement-dependent cytotoxicity, inducing immune mechanisms to exert anti-tumor effects. Auner HW found that sustained high levels of antibody secretion by plasma cells lead to secretion overload and ER stress [65]. Interestingly, activation of key apoptotic caspases was blocked in plasma cells, and excessive ER stress was the main cause of plasma cell death. Additionally, Kang W found that in the poor prognostic autophagy-related subtype of NB, the infiltration level of B cell was significantly increased, and there was a close association between cellular autophagy and ER stress [66]. Therefore, the high-risk ERSRsubtype of NB may adapt to ER stress to resist the death of B cells. These findings are consistent with our results. T cells CD8 and T cells CD4, as important components of cellular immunity, play roles in direct killing of tumor cells and assisting in anti-tumor immunity, respectively, and are the main effector cells in tumor immune responses. This link between immune phenotype and clinical risk extends the relevance of tumor-immune crosstalk beyond NB, aligning with established prognostic immune signatures in other neural tumors like glioma [67]. Fernández-Alfara M found that *CPEB4* was required for T cell effector function and was induced in effector TILs and activated CD8<sup>+</sup> T cells [68]. Depletion of *CPEB4* in T lymphocytes impairs T cell-mediated anti-tumor immunity and exacerbates terminal UPR in activated CD8<sup>+</sup> T cells [68]. This study also found that in the poor prognostic ERSRsubtype, the expression level of *CPEB4* was significantly increased. Therefore, low expression of *CPEB4* may lead to the inability of activated CD8<sup>+</sup> T cells to adapt to ER stress and undergo apoptosis. Mitochondrial reactive oxygen species are a hallmark of mitochondrial exhaustion in T cells. Hurst KE found that PERK contributed to the activation of chronic ER stress in T effector cells by consuming energy in CD8<sup>+</sup> T effector cells [69]. Tumor antigen-specific PD-1<sup>+</sup> CD8<sup>+</sup>

tumor-infiltrating lymphocytes exhibit mitochondrial exhaustion, and PERK inhibition improves anti-PD-1 therapy [69]. Therefore, ER stress inhibitors have a significant promoting effect on the tumor-killing ability of CD8<sup>+</sup> T cells. T cells CD4 memory resting are generated in numerous infection modalities and can play protective roles. Additionally, T cells CD4 memory resting have been found to play roles in various autoimmune diseases. The identification of human tissue-resident memory T cells in non-transplant settings is challenging, especially relying on the imperfect surface marker CD69 [70]. Therefore, there is still a need for technological improvements to accurately identify CD4 memory resting T cells. The mechanism of T cells CD4 memory resting in ER stress is still unclear, and there is currently no research on this in NB. This makes T cells CD4 memory resting a type of immune cell that requires further research. More studies are needed to investigate how they function in the TME of NB.

Herein, we report the first systematic identification of molecular subtypes in NB based on ERSRGs, revealing their significant associations with patient prognosis and key clinical characteristics. This work advances beyond the general recognition of ER stress in cancer by specifically contextualizing and mechanistically substantiating its role within NB biology. We demonstrated that NB exhibits pronounced heterogeneity in its ER stress response, which directly translates to a clinically meaningful prognostic stratification. Notably, the 10-gene ER stress related prognostic signature developed in this study offers value extending beyond an alternative predictive metric. We posit that its core utility lies in providing complementary information and a novel clinical perspective that enhances current mainstream biomarkers. First, this model serves as a significant complement to the established, single-gene *MYCN* centric risk stratification. While *MYCN* amplification remains a cornerstone high-risk marker, its predictive power is not absolute. Our signature retained independent prognostic value in multivariate analysis, indicating it captures pathogenic pathway information not fully encompassed by *MYCN* status. Crucially, within the *MYCN* amplified cohort itself, a high-risk score was associated with inferior outcomes, suggesting its potential to refine high-risk patient classification and identify subsets warranting more intensive intervention. Second, the model integrates TME information from an upstream mechanistic vantage point. Although immune cell infiltration-based scores have prognostic merit, our signature is derived from an intrinsic tumor cell process, ER stress, that is a known driver of TME remodeling. The distinct immune infiltration landscapes observed between risk groups, along with correlations between signature genes and specific immune cell abundances, suggest that our risk score

concurrently reflects the intrinsic stress state of tumor cells and their capacity to shape the immune milieu. This offers a predictive dimension with greater mechanistic explanatory power. Finally, and most critically for translational potential, the model provides biologically informed therapeutic clues. Traditional staging and *MYCN* status primarily guide chemotherapy intensity but offer limited direction for targeted or optimized drug selection. Our signature-based drug sensitivity analysis pinpointed 18 chemotherapeutic agents predicted to exhibit greater efficacy in the high-risk group. This directly links the ERSRG derived molecular subtype with potential therapeutic vulnerabilities, providing a rationale for exploring personalized, pathway-informed combination strategies for high-risk or refractory NB. This aligns with the emerging paradigm of risk-guided pharmacotyping for precision oncology [71]. Thus, the signature holds promise for evolving from a prognostic tool into an aid for therapeutic decision-making.

## Conclusion

In conclusion, we have revealed that there are two distinct ERSRsubtypes of NB with significant differences in prognosis through this study. These subtypes exhibit clear distinctions in terms of clinical symptoms, signaling pathways, TME and so on. Furthermore, this research has established an accurate, effective, and widely applicable predictive ER stress related model for NB. Future work should focus on validating the robustness of this model in independent, prospective cohorts and further investigating the predicted candidate drugs in preclinical models. The ultimate goal is to translate the biology of ER stress into tangible strategies for improving the clinical management of NB patients.

## Supplementary Information

The online version contains supplementary material available at <https://doi.org/10.1186/s12885-026-15774-0>.

Additional file 1.

Additional file 2.

Additional file 3.

Additional file 4.

Additional file 5.

Additional file 6: The 18 kinds of drugs predicted to be the most sensitive to the high risk group.

Additional file 7: The 131 kinds of drugs predicted to be the most sensitive to the low risk group.

Additional file 8: Table S1. The sequences of primers for qRT-PCR.

Additional file 9: Table S2. shRNA sequences.

Additional file 10: Figure S1. The distribution differences of clinical traits between different ERSRclusters and risk groups. A-E The distribution levels of age  $\geq 18$  months, high COG risk, and INSS stage III-IV were higher in ERSRcluster B ( $p < 0.0001$ ). *MYCN* amplified was completely distributed

in ERSRcluster B. There was no difference in the distribution of gender between the two clusters ( $p > 0.05$ ). F-J The distribution levels of age  $\geq 18$  months, *MYCN* amplified, high COG risk, and INSS stage III-IV were higher in high risk group ( $p < 0.0001$ ). There was no difference in the distribution of gender between the two risk groups ( $p > 0.05$ ). ERSRcluster, ER stress related cluster; COG, Children's Oncology Group; INSS, international neuroblastoma staging system.

## Acknowledgements

We express our thanks to the public databases for furnishing us with data, and to the developers of R software and R packages for their contributions and convenience.

## Authors' contributions

BD, BJ and LH proposed the idea of the article and supervised its completion. JC drafted and reviewed the article. JC performed the bioinformatics analysis. BD and BJ helped to interpret the data and prepare the figures. All authors read and approved the final manuscript.

## Funding

This research was funded by Nanjing Medical Science and Technology Development Project, grant number YKK24155.

## Data availability

All the data used in the current study are available in GEO (<https://www.ncbi.nlm.nih.gov/geo/>) (accessed on 20 October 2025) and TARGET (<https://portal.gdc.cancer.gov/>) (accessed on 20 October 2025) repositories.

## Declarations

### Ethics approval and consent to participate

Not applicable.

### Consent for publication

Not applicable.

### Competing interests

The authors declare no competing interests.

Received: 27 November 2025 / Accepted: 16 February 2026

Published online: 03 March 2026

## References

1. Ni X, Li Z, Li X, Zhang X, Bai G, Liu Y, Zheng R, Zhang Y, Xu X, Liu Y, et al. Socioeconomic inequalities in cancer incidence and access to health services among children and adolescents in China: a cross-sectional study. *Lancet*. 2022;400:1020–32.
2. Irwin MS, Naranjo A, Zhang FF, Cohn SL, London WB, Gastier-Foster JM, Ramirez NC, Pfau R, Reshmi S, Wagner E, et al. Revised Neuroblastoma Risk Classification System: A Report From the Children's Oncology Group. *J Clin Oncol*. 2021;39:3229–41.
3. Pinto N, Naranjo A, Ding X, Zhang FF, Hibbitts E, Kennedy R, Tibbitts R, Wong-Michalak S, Craig DW, Manojlovic Z, et al. Impact of Genomic and Clinical Factors on Outcome of Children  $\geq 18$  Months of Age with Stage 3 Neuroblastoma with Unfavorable Histology and without *MYCN* Amplification: A Children's Oncology Group (COG) Report. *Clin Cancer Res*. 2023;29:1546–56.
4. Sokol E, Desai AV, Applebaum MA, Valteau-Couanet D, Park JR, Pearson ADJ, Schleiermacher G, Irwin MS, Hogarty M, Naranjo A, et al. Age, Diagnostic Category, Tumor Grade, and Mitosis-Karyorrhexis Index Are Independently Prognostic in Neuroblastoma: An INRG Project. *J Clin Oncol*. 2020;38:1906–18.
5. Strother DR, London WB, Schmidt ML, Brodeur GM, Shimada H, Thorner P, Collins MH, Tagge E, Adkins S, Reynolds CP, et al. Outcome after surgery alone or with restricted use of chemotherapy for patients with low-risk neuroblastoma: results of Children's Oncology Group study P9641. *J Clin Oncol*. 2012;30:1842–8.
6. Berthold F, Faldum A, Ernst A, Boos J, Dilloo D, Eggert A, Fischer M, Frühwald M, Henze G, Klingebiel T, et al. Extended induction chemotherapy does not

- improve the outcome for high-risk neuroblastoma patients: results of the randomized open-label GPOH trial NB2004-HR. *Ann Oncol.* 2020;31:422–9.
7. Garaventa A, Poetschger U, Valteau-Couanet D, Luksch R, Castel V, Elliott M, Ash S, Chan GCF, Laureys G, Beck-Popovic M, et al. Randomized Trial of Two Induction Therapy Regimens for High-Risk Neuroblastoma: HR-NBL1.5 International Society of Pediatric Oncology European Neuroblastoma Group Study. *J Clin Oncol.* 2021;39:2552–63.
  8. Campbell K, Groshen S, Evans AC, Wilson S, Sebastian A, Loots GG, Marachevian A, Armant M, Pal S, Haas-Kogan DA, et al. Modulation of Radiation Biomarkers in a Randomized Phase II Study of (131)I-MIBG With or Without Radiation Sensitizers for Relapsed or Refractory Neuroblastoma. *Int J Radiat Oncol Biol Phys.* 2023;115:1115–28.
  9. Gains JE, Patel A, Chang YC, Mandeville HC, Smyth G, Stacey C, Talbot J, Wheatley K, Gaze MN. A Randomised Phase II Trial to Evaluate the Feasibility of Radiotherapy Dose Escalation, Facilitated by Intensity-Modulated Arc Radiotherapy Techniques, in High-Risk Neuroblastoma. *Clin Oncol (R Coll Radiol).* 2024;36:e154–62.
  10. Park JR, Kreissman SG, London WB, Naranjo A, Cohn SL, Hogarty MD, Tenney SC, Haas-Kogan D, Shaw PJ, Kravaka JM, et al. Effect of Tandem Autologous Stem Cell Transplant vs Single Transplant on Event-Free Survival in Patients With High-Risk Neuroblastoma: A Randomized Clinical Trial. *JAMA.* 2019;322:746–55.
  11. Kuroda R, Wakabayashi H, Araki R, Inaki A, Nishimura R, Ikawa Y, Yoshimura K, Murayama T, Imai Y, Funasaka T, et al. Phase I/II clinical trial of high-dose [(131)I] meta-iodobenzylguanidine therapy for high-risk neuroblastoma preceding single myeloablative chemotherapy and haematopoietic stem cell transplantation. *Eur J Nucl Med Mol Imaging.* 2022;49:1574–83.
  12. Flaadt T, Ladenstein RL, Ebinger M, Lode HN, Arnardóttir HB, Poetschger U, Schwinger W, Meisel R, Schuster FR, Döring M, et al. Anti-GD2 Antibody Dinutuximab Beta and Low-Dose Interleukin 2 After Haploidentical Stem-Cell Transplantation in Patients With Relapsed Neuroblastoma: A Multicenter, Phase I/II Trial. *J Clin Oncol.* 2023;41:3135–48.
  13. Heczey A, Xu X, Courtney AN, Tian G, Barragan GA, Guo L, Amador CM, Ghatwai N, Rath P, Wood MS, et al. Anti-GD2 CAR-NKT cells in relapsed or refractory neuroblastoma: updated phase 1 trial interim results. *Nat Med.* 2023;29:1379–88.
  14. Gargett T, Truong NTH, Gardam B, Yu W, Ebert LM, Johnson A, et al. Safety and biological outcomes following a phase 1 trial of GD2-specific CAR-T cells in patients with GD2-positive metastatic melanoma and other solid cancers. *J Immunother Cancer.* 2024;12:e008659.
  15. Yankelevich M, Thakur A, Modak S, Chu R, Taub J, Martin A, et al. Targeting refractory/recurrent neuroblastoma and osteosarcoma with anti-CD3xanti-GD2 bispecific antibody armed T cells. *J Immunother Cancer.* 2024;12:e008744.
  16. Liu Y, Xu C, Gu R, Han R, Li Z, Xu X. Endoplasmic reticulum stress in diseases. *MedComm (2020).* 2024;5:e701.
  17. Zhang W, Shi Y, Oyang L, Cui S, Li S, Li J, Liu L, Li Y, Peng M, Tan S, et al. Endoplasmic reticulum stress—a key guardian in cancer. *Cell Death Discov.* 2024;10:343.
  18. Oakes SA. Endoplasmic Reticulum Stress Signaling in Cancer Cells. *Am J Pathol.* 2020;190:934–46.
  19. Unal B, Kuzu OF, Jin Y, Osorio D, Kildal W, Pradhan M, Kung SHY, Oo HZ, Daugaard M, Vendelbo M, et al. Targeting IRE1α reprograms the tumor microenvironment and enhances anti-tumor immunity in prostate cancer. *Nat Commun.* 2024;15:8895.
  20. Chen Q, Li C, Wei W, Li J, Liu F, Fu Y, Tang L, Han F. Endoplasmic reticulum stress response pathway-mediated cell death in ovarian cancer. *Front Oncol.* 2024;14:1446552.
  21. Zhao Y, Wu X, Meng F, Liu X, Yuan J, Zhang X, Tian G, Wu X. ER stress-induced LINC00173 promotes the apoptosis of ovarian granulosa cells by regulating the HRK/PI3K/AKT pathway in polycystic ovary syndrome. *Sci Rep.* 2024;14:24636.
  22. Wang J, Zhang Z, Zhuo Y, Zhang Z, Chen R, Liang L, Jiang X, Nie D, Liu C, Zou Z, et al. Endoplasmic reticulum-targeted delivery of celastrol and PD-L1 siRNA for reinforcing immunogenic cell death and potentiating cancer immunotherapy. *Acta Pharm Sin B.* 2024;14:3643–60.
  23. Böhme R, Schmidt AW, Hesselbarth N, Posern G, Sinz A, Ihling C, Michl P, Laumen H, Rosendahl J. Induction of oxidative- and endoplasmic-reticulum-stress dependent apoptosis in pancreatic cancer cell lines by DDOST knock-down. *Sci Rep.* 2024;14:20388.
  24. Pecoraro M, Serra A, Pascale M, Franceschelli S. The ER Stress Induced in Human Neuroblastoma Cells Can Be Reverted by Lumacaftor, a CFTR Corrector. *Curr Issues Mol Biol.* 2024;46:9342–58.
  25. Lochmann TL, Powell KM, Ham J, Floros KV, Heisey DAR, Kurupi RJ, et al. Targeted inhibition of histone H3K27 demethylation is effective in high-risk neuroblastoma. *Sci Transl Med.* 2018;10:eaa04680.
  26. Duan WW, Yang LT, Liu J, Dai ZY, Wang ZY, Zhang H, Zhang X, Liang XS, Luo P, Zhang J, et al. A TGF-β signaling-related lncRNA signature for prediction of glioma prognosis, immune microenvironment, and immunotherapy response. *CNS Neurosci Ther.* 2024;30:e14489.
  27. Tibshirani R. The lasso method for variable selection in the Cox model. *Stat Med.* 1997;16:385–95.
  28. Xie Y, Wang M, Qian Y, Li L, Sun Q, Gao M, Li C. Novel PdPtCu Nanozymes for Reprogramming Tumor Microenvironment to Boost Immunotherapy Through Endoplasmic Reticulum Stress and Blocking IDO-Mediated Immune Escape. *Small.* 2023;19:e2303596.
  29. Salvagno C, Mandula JK, Rodriguez PC, Cubillos-Ruiz JR. Decoding endoplasmic reticulum stress signals in cancer cells and antitumor immunity. *Trends Cancer.* 2022;8:930–43.
  30. Wei W, Zhang Y, Song Q, Zhang Q, Zhang X, Liu X, Wu Z, Xu X, Xu Y, Yan Y, et al. Transmissible ER stress between macrophages and tumor cells configures tumor microenvironment. *Cell Mol Life Sci.* 2022;79:403.
  31. Baluapuri A, Wolf E, Eilers M. Target gene-independent functions of MYC oncoproteins. *Nat Rev Mol Cell Biol.* 2020;21:255–67.
  32. Chipmuro E, Marco E, Christensen CL, Kwiatkowski N, Zhang T, Hatheway CM, Abraham BJ, Sharma B, Yeung C, Altabef A, et al. CDK7 inhibition suppresses super-enhancer-linked oncogenic transcription in MYCN-driven cancer. *Cell.* 2014;159:1126–39.
  33. Herold S, Kalb J, Büchel G, Ade CP, Baluapuri A, Xu J, Koster J, Solvie D, Carstensen A, Klotz C, et al. Recruitment of BRCA1 limits MYCN-driven accumulation of stalled RNA polymerase. *Nature.* 2019;567:545–9.
  34. Chen X, Cubillos-Ruiz JR. Endoplasmic reticulum stress signals in the tumour and its microenvironment. *Nat Rev Cancer.* 2021;21:71–88.
  35. Lan Z, Tan F, He J, Liu J, Lu M, Hu Z, Zhuo Y, Liu J, Tang X, Jiang Z, et al. Curcumin-primed olfactory mucosa-derived mesenchymal stem cells mitigate cerebral ischemia/reperfusion injury-induced neuronal PANoptosis by modulating microglial polarization. *Phytomedicine.* 2024;129:155635.
  36. Ma Y, Yang H, Pitt JM, Kroemer G, Zitvogel L. Therapy-induced microenvironmental changes in cancer. *J Mol Med (Berl).* 2016;94:497–508.
  37. Zhang J, Pavlova NN, Thompson CB. Cancer cell metabolism: the essential role of the nonessential amino acid, glutamine. *Embo j.* 2017;36:1302–15.
  38. de Almeida SF, Fleming JV, Azevedo JE, Carmo-Fonseca M, de Sousa M. Stimulation of an unfolded protein response impairs MHC class I expression. *J Immunol.* 2007;178:3612–9.
  39. Xu L, Peng F, Luo Q, Ding Y, Yuan F, Zheng L, et al. IRE1α silences dsRNA to prevent taxane-induced pyroptosis in triple-negative breast cancer. *Cell.* 2024;187:7248–66.e34.
  40. Hu J, Chen NN, Li LG, Yu TT, Qin Y, Peng XC, Li HT, Li XY, Ma TQ, Lu YH, et al. Cepharanthine-mediated endoplasmic reticulum stress inhibits Notch1 via binding GRP78 for suppressing hepatocellular carcinoma metastasis. *Phyto-medicine.* 2024;135:156162.
  41. Liu Y, Lin W, Qian H, Yang Y, Zhou X, Wu C, Pan X, Liu Y, Wang G. Integrated multi-omic analysis and experiment reveals the role of endoplasmic reticulum stress in lung adenocarcinoma. *BMC Med Genomics.* 2024;17:12.
  42. Zheng Y, Yue X, Fang C, Jia Z, Chen Y, Xie H, Zhao J, Yang Z, Li L, Chen Z, et al. A Novel Defined Endoplasmic Reticulum Stress-Related lncRNA Signature for Prognosis Prediction and Immune Therapy in Glioma. *Front Oncol.* 2022;12:930923.
  43. Zhao P, Zhen H, Zhao H, Huang Y, Cao B. Identification of hub genes and potential molecular mechanisms related to radiotherapy sensitivity in rectal cancer based on multiple datasets. *J Transl Med.* 2023;21:176.
  44. Tao J, Yin L, Wu A, Zhang J, Zhang J, Shi H, Liu S, Niu L, Xu L, Feng Y, et al. PDIA2 Bridges Endoplasmic Reticulum Stress and Metabolic Reprogramming During Malignant Transformation of Chronic Colitis. *Front Oncol.* 2022;12:836087.
  45. Zhao X, Liu X, Su L. Parthenolide induces apoptosis via TNFRSF10B and PMAIP1 pathways in human lung cancer cells. *J Exp Clin Cancer Res.* 2014;33:3.
  46. Liu Y, Meng X, Tang C, Zheng L, Tao K, Guo W. Aerobic exercise modulates RIPK1-mediated MAP3K5/JNK and NF-κB pathways to suppress microglia activation and neuroinflammation in the hippocampus of D-gal-induced accelerated aging mice. *Physiol Behav.* 2024;286:114676.

47. Benedetti R, Romeo MA, Arena A, Gilardini Montani MS, D'Orazi G, Cirone M. ATF6 supports lysosomal function in tumor cells to enable ER stress-activated macroautophagy and CMA: impact on mutant TP53 expression. *Autophagy*. 2024;20:1854–67.
48. Lin WC, Chuang YC, Chang YS, Lai MD, Teng YN, Su IJ, Wang CC, Lee KH, Hung JH. Endoplasmic reticulum stress stimulates p53 expression through NF- $\kappa$ B activation. *PLoS ONE*. 2012;7:e39120.
49. Zhang T, Li N, Sun C, Jin Y, Sheng X. MYC and the unfolded protein response in cancer: synthetic lethal partners in crime? *EMBO Mol Med*. 2020;12:e11845.
50. Xie H, Tang CH, Song JH, Mancuso A, Del Valle JR, Cao J, Xiang Y, Dang CV, Lan R, Sanchez DJ, et al. IRE1 $\alpha$  RNase-dependent lipid homeostasis promotes survival in Myc-transformed cancers. *J Clin Invest*. 2018;128:1300–16.
51. Tameire F, Verginadis II, Leli NM, Polte C, Conn CS, Ojha R, Salas Salinas C, Chinga F, Monroy AM, Fu W, et al. ATF4 couples MYC-dependent translational activity to bioenergetic demands during tumour progression. *Nat Cell Biol*. 2019;21:889–99.
52. Langfelder P, Horvath S. WGCNA: an R package for weighted correlation network analysis. *BMC Bioinformatics*. 2008;9:559.
53. Jiao B, Zhang M, Zhang C, Cao X, Liu B, Li N, Sun J, Zhang X. Transcriptomics reveals the effects of NTRK1 on endoplasmic reticulum stress response-associated genes in human neuronal cell lines. *PeerJ*. 2023;11:e15219.
54. Wang S, Cheng Z, Cui Y, Xu S, Luan Q, Jing S, Du B, Li X, Li Y. PTPRH promotes the progression of non-small cell lung cancer via glycolysis mediated by the PI3K/AKT/mTOR signaling pathway. *J Transl Med*. 2023;21:819.
55. Lee HS, Kim EN, Jeong GS. Aromadendrin protects neuronal cells from Methamphetamine-Induced Neurotoxicity by regulating endoplasmic reticulum stress and PI3K/Akt/mTOR signaling pathway. *Int J Mol Sci*. 2021;22:2274.
56. Zhou R, Lu Z, Luo H, Xiang J, Zeng M, Li M. NEDD: a network embedding based method for predicting drug-disease associations. *BMC Bioinformatics*. 2020;21:387.
57. Guo YF, Duan JJ, Wang J, Li L, Wang D, Liu XZ, et al. Inhibition of the ALDH18A1-MYCN positive feedback loop attenuates MYCN-amplified neuroblastoma growth. *Sci Transl Med*. 2020;12:eaax8694.
58. Gong T, Wang Q, Lin Z, Chen ML, Sun GZ. Endoplasmic reticulum (ER) stress inhibitor salubrinal protects against ceramide-induced SH-SY5Y cell death. *Biochem Biophys Res Commun*. 2012;427:461–5.
59. Thomas CG, Spyrou G. ERdj5 sensitizes neuroblastoma cells to endoplasmic reticulum stress-induced apoptosis. *J Biol Chem*. 2009;284:6282–90.
60. Carén H, Holmstrand A, Sjöberg RM, Martinsson T. The two human homologues of yeast UFD2 ubiquitination factor, UBE4A and UBE4B, are located in common neuroblastoma deletion regions and are subject to mutations in tumours. *Eur J Cancer*. 2006;42:381–7.
61. Xing Z, Yan J, Miao Y, Ruan Y, Yao H, Zhou Y, Tang Y, Li G, Song Z, Peng Y, et al. Endoplasmic Reticulum-Targeting Quinazolinone-Based Lipophilic Probe for Specific Photoinduced Ferroptosis and Its Induced Lipid Dynamic Regulation. *J Med Chem*. 2024;67:1900–13.
62. Wouters MCA, Nelson BH. Prognostic Significance of Tumor-Infiltrating B Cells and Plasma Cells in Human Cancer. *Clin Cancer Res*. 2018;24:6125–35.
63. Patil NS, Nabet BY, Müller S, Koeppen H, Zou W, Giltne J, Au-Yeung A, Srivats S, Cheng JH, Takahashi C, et al. Intratumoral plasma cells predict outcomes to PD-L1 blockade in non-small cell lung cancer. *Cancer Cell*. 2022;40:289–e300284.
64. Hu J, Zhang L, Xia H, Yan Y, Zhu X, Sun F, Sun L, Li S, Li D, Wang J, et al. Tumor microenvironment remodeling after neoadjuvant immunotherapy in non-small cell lung cancer revealed by single-cell RNA sequencing. *Genome Med*. 2023;15:14.
65. Auner HW, Beham-Schmid C, Dillon N, Sabbattini P. The life span of short-lived plasma cells is partly determined by a block on activation of apoptotic caspases acting in combination with endoplasmic reticulum stress. *Blood*. 2010;116:3445–55.
66. Kang W, Hu J, Zhao Q, Song F. Identification of an Autophagy-Related Risk Signature Correlates With Immunophenotype and Predicts Immune Checkpoint Blockade Efficacy of Neuroblastoma. *Front Cell Dev Biol*. 2021;9:731380.
67. Zeng WJ, Zhang L, Cao H, Li D, Zhang H, Xia Z, Peng R. A novel inflammation-related lncRNAs prognostic signature identifies LINC00346 in promoting proliferation, migration, and immune infiltration of glioma. *Front Immunol*. 2022;13:810572.
68. Fernández-Alfara M, Sibilio A, Martin J, Tusquets Uxó E, Malumbres M, Alcalde V, Chanes V, Cañellas-Socias A, Palomo-Ponce S, Battle E, Méndez R. Antitumor T-cell function requires CPEB4-mediated adaptation to chronic endoplasmic reticulum stress. *Embo j*. 2023;42:e111494.
69. Hurst KE, Lawrence KA, Essman MT, Walton ZJ, Leddy LR, Thaxton JE. Endoplasmic Reticulum Stress Contributes to Mitochondrial Exhaustion of CD8(+) T Cells. *Cancer Immunol Res*. 2019;7:476–86.
70. Wiggins BG, Pallett LJ, Li X, Davies SP, Amin OE, Gill US, Kucykowicz S, Patel AM, Aliasis K, Liu YS, et al. The human liver microenvironment shapes the homing and function of CD4(+) T-cell populations. *Gut*. 2022;71:1399–411.
71. Li J, He HG, Guan C, Ding Y, Hu X. Dynamic joint prediction model of severe radiation-induced oral mucositis among nasopharyngeal carcinoma: a prospective longitudinal study. *Radiother Oncol*. 2025;209:110993.

## Publisher's note

Springer Nature remains neutral with regard to jurisdictional claims in published maps and institutional affiliations.